Identification of novel buffering mechanisms in aortic arch artery development and congenital heart disease

AnnJosette Ramirez[1,2], Karl Degenhardt[4], and Sophie Astrof[1,2,3*]

1. Department of Cell Biology and Molecular Medicine, New Jersey Medical School, Rutgers Biomedical and Health Sciences, Newark, NJ, 07103

2. Multidisciplinary Ph.D. Program in Biomedical Sciences: Cell Biology, Neuroscience and Physiology Track, New Jersey Medical School, Rutgers Biomedical and Health Sciences, Newark, NJ, 07103

3. Multidisciplinary Ph.D. Program in Biomedical Sciences: Molecular Biology, Genetics, and Cancer Track, New Jersey Medical School, Rutgers Biomedical and Health Sciences, Newark, NJ, 07103

4. Children's Hospital of Pennsylvania, University of Pennsylvania, Philadelphia, PA 19107

* Author for correspondence

Sophie Astrof (sophie.astrof@rutgers.edu)

Summary

The remarkable robustness of embryonic development to genetic and environmental perturbations has been long appreciated; however, little is known about buffering mechanisms underlying the constancy of development. Yet, aberrations in developmental programs can lead to lethal outcomes, exemplified by congenital heart disease (CHD). Defective morphogenesis of the aortic arch is a lethal CHD phenotype common in 22q11 deletion syndrome (22q11DS). Previously, we found that the second heart field (SHF) gives rise to the pharyngeal arch artery (PAA) endothelium. Here, we show that robust PAA development is dependent on both a threshold and an optimum number of SHF-derived endothelial cells (ECs) and that the optimum number is regulated by *VEGFR2* and *Tbx1* gene dosage. We discovered that when the number of SHF-derived ECs falls below the optimum but remains within the threshold, PAA development is rescued by a compensatory endothelium. To determine the source of compensating endothelium and the mechanisms regulating its recruitment, we used *in toto* confocal imaging to investigate EC connectivity, fate, and gene expression at single-cell and single-molecule resolutions. Our studies demonstrate that the loss of SHF-derived ECs leads to alterations in the pharyngeal tissue microenvironment, resulting in increased synthesis of *VEGFA*, eliciting ectopic angiogenesis from the nearby veins but not arteries. We show that this rescuing mechanism is regulated by *Tbx1*, a major 22q11DS disease gene; the absence of a single allele of *Tbx1* prevents this angiogenic response leading to unpredictable arch artery morphogenesis and lethal CHD in *Tbx1*$^{+/-}$ animals. Together, our work uncovers a novel buffering mechanism underlying the fidelity of arch artery development and provides insights into the pathogenesis of CHD.

Introduction

How complex developmental processes almost invariably lead to predictable phenotypes has remained a conundrum for many years. In 1942, C.H. Waddington proposed the concept of canalization of development, which refers to the tendency of developmental processes to follow a specific trajectory despite genetic and environmental perturbations (Waddington, 1942). Noting that genetically "wild type" organisms have much less developmental variability than organisms with genetic mutations, Waddington argued for a buffering mechanism(s) that allow constancy in developmental outcomes despite minor genetic or environmental perturbations. One example of canalized development is the organogenesis of the cardiovascular system. The aortic arch is a major vessel that circulates oxygenated blood throughout the body. In wild-type mice and humans, this vessel forms a leftward arch to connect the heart and the descending aorta. However, mutations affecting pharyngeal mesoderm or cardiac neural crest development can result in unpredictable defects in arch artery development and remodeling; the aortic arch can form a rightward arch, form two arches, or be absent completely (Stoller and Epstein, 2005). Although rare, congenital defects offer an opportunity to understand buffering mechanisms underlying the constancy of developmental outcomes and their alterations resulting in birth defects.

Congenital heart disease (CHD) is the most prevalent congenital anomaly, affecting approximately 8 per 1000 live births in the United States (Benjamin et al., 2018; Tsao et al., 2022). Defects in the development of the aorta, aortic arch arteries (AAAs), and pulmonary trunk give rise to the most severe forms of CHD. The aortic arch and AAAs are derived from three bilateral pairs of pharyngeal arch arteries (PAAs), namely the 3rd, 4th, and 6th. During development, nascent PAAs undergo asymmetric remodeling to give rise to mature AAAs (Kau et al., 2007; Stoller and Epstein, 2005). Defective formation and remodeling of the left 4th PAA leads to the lethal CHD phenotype interrupted aortic arch type B (IAA-B), resulting in the loss of luminal continuity between the ascending and descending aorta and interrupting the circulation of the oxygenated blood throughout the body (Celoria and Patton, 1959). Improper formation and remodeling of the right 4th PAA results in the non-lethal CHD phenotype retro-esophageal right subclavian artery (RERSA), where the right subclavian artery branches from the descending aorta. Although a non-lethal CHD phenotype, RERSA can lead to dysphagia lusoria (Levitt and Richter, 2007).

71 Chromosome 22q11 deletion syndrome (22q11 DS) is one of the most prevalent chromosomal
72 microdeletion syndromes, with an incidence of 1 in 3,000-6,000 live births (McDonald-McGinn
73 and Sullivan, 2011; McDonald-McGinn et al., 2015). Characterized by multiple anomalies, 80%
74 of 22q11DS cases present with congenital heart disease (McDonald-McGinn et al., 2015;
75 Momma, 2010). Further, approximately 50-60% of patients with interrupted aortic arch have
76 22q11DS, with IAA-B being the most prevalent subtype (Collins-Nakai et al., 1976; Goldmuntz et
77 al., 1993; Moerman et al., 1987; Van Mierop and Kutsche, 1986b). *Tbx1* is among the genes
78 deleted in 22q11DS, and knockout studies demonstrated that heterozygosity of *Tbx1* in mice
79 results in aberrant 4th PAA development and phenocopies 4th PAA-derived aortic arch defects in
80 22q11DS patients (Jerome and Papaioannou, 2001; Lindsay et al., 2001; Merscher et al., 2001).

81 The PAAs develop within pharyngeal arches, a series of bulges on the lateral surface of the
82 thoracic region of the embryo (Graham, 2003). PAAs form by vasculogenesis, where mesoderm-
83 derived vascular progenitors populate the pharyngeal arches and differentiate into endothelial
84 cells (ECs). These endothelial cells form a primary network of small vessels which then coalesce
85 into a patent artery (Li et al., 2012; Nagelberg et al., 2015; Paffett-Lugassy et al., 2013; Wang et
86 al., 2017; Warkala et al., 2021). We and others have previously shown that PAA endothelium,
87 particularly the 4th and 6th PAAs, is mainly derived from a subpopulation of splanchnic mesoderm
88 known as the Second Heart Field (SHF) (Paffett-Lugassy et al., 2013; Wang et al., 2017; Warkala
89 et al., 2021). However, the role of SHF-derived vascular progenitors in PAA morphogenesis, the
90 mechanisms regulating their contribution to the PAAs, and the impact of *Tbx1* haploinsufficiency
91 on this process are unknown.

92 To investigate the developmental mechanisms regulating PAA formation and remodeling, we
93 used transgenic mouse models to manipulate the expression of *VEGFR2* and *Tbx1*. Our findings
94 demonstrate that the correct *VEGFR2* gene dosage in the SHF is crucial for the contribution of
95 SHF-derived ECs to the PAA endothelium. We show that robust arch artery development requires
96 both a threshold and an optimum number of SHF-derived endothelial cells (ECs). The expression
97 of *VEGFR2* and *Tbx1* regulates this optimum number in a dosage-dependent manner.
98 Furthermore, we discovered that when the number of SHF-derived endothelium falls below the
99 optimum, the arch artery can be rebuilt from endothelial cells that arise from nearby veins via
100 angiogenesis. This angiogenic response is suppressed when the optimum number of SHF-
101 derived endothelial cells is present in the pharyngeal arches. However, when the number of SHF-
102 derived ECs falls below the optimum, the pharyngeal tissue microenvironment is altered, resulting
103 in increased synthesis of VEGFA in the pharyngeal arches. Of significant importance for human

disease, the buffering capacity during arch artery development is regulated by *Tbx1* in a dosage-dependent manner, which mediates the recruitment of venous endothelium by regulating angiogenic sprouting from veins. Altogether, this work provides insights into buffering mechanisms underlying robustness and plasticity in the development of the aortic arch.

Results

The expression of VEGFR2 in the SHF is required for the specification of pharyngeal arch endothelium.

To determine whether the SHF is a principal source of the PAA endothelium, we ablated VEGFR2 from the SHF using the *Isl1*^{Cre} knock-in strain by crossing *VEGFR2*$^{+/-}$*;Isl1*$^{Cre/+}$ mice with *VEGFR2*$^{f/f}$*;Rosa*$^{mTmG/mTmG}$ mice, generating *VEGFR2*$^{flox/-}$*;Isl1*$^{Cre/+}$ (*VEGFR2*$^{Isl1\text{-}KO}$), *VEGFR2*$^{flox/+}$*;Isl1*$^{Cre/+}$ (*VEGFR2*$^{Isl1\text{-}Het}$), and *VEGFR2*$^{flox/+}$*;Isl1*$^{+/+}$ (*VEGFR2*$^{Isl1\text{-}WT}$) embryos. Embryos were examined at embryonic day (E) 10.5 when PAA formation was nearly complete (34 – 36s) (Anderson and Bamforth, 2022; Wang et al., 2017; Warkala et al., 2021). Vasculature was visualized using whole-mount immunofluorescent staining (WM-IF) and antibodies against VEGFR2, followed by confocal imaging of the entire pharyngeal region and three-dimensional (3D) reconstruction of optical sections. We hypothesized that the deletion of VEGFR2 from the SHF would result in the absence of PAA endothelium and that no PAAs would form. Our analyses showed that PAA formation in *VEGFR2*$^{Isl1\text{-}Het}$ and *VEGFR2*$^{Isl1\text{-}KO}$ embryos was defective, compared to *VEGFR2*$^{Isl1\text{-}WT}$ (**Fig. S1)**; the 6th PAA of *VEGFR2*$^{Isl1\text{-}Het}$ embryos was hypoplastic (compare **Fig. S1A-B** with **Fig. S1C-D**), whereas the 4th and 6th PAAs of *VEGFR2*$^{Isl1\text{-}KO}$ embryos were either hypoplastic or aplastic (**Fig. S1E-F, Table S1**). Surprisingly, despite the downregulation of VEGFR2 from the SHF (**Fig. S1G-I, outlined**), VEGFR2+ endothelium was present in all three pharyngeal arches of *VEGFR2*$^{Isl1\text{-}KO}$ embryos (**Fig. S1E-F**). These results suggest that either VEGFR2 expression is not essential for the differentiation of SHF-derived vascular progenitors into PAA ECs or that the endothelium in the mutant embryos was derived from a source other than the SHF.

To test these hypotheses and determine the fate of SHF-derived mesoderm in mutant embryos, we used the *mef2c-AHF-Cre* and *Rosa*^{tdTomato} strains. For these experiments, *VEGFR2*$^{+/-}$*;mef2c-AHF-Cre* mice were crossed with *VEGFR2*$^{flox/flox}$;*Rosa*$^{tdTom/tdTom}$ mice to generate *VEGFR2*$^{flox/-}$*;mef2c-AHF-Cre+;Rosa*$^{tdTom/+}$ (*VEGFR2*$^{SHF\text{-}KO}$) embryos and *VEGFR2*$^{flox/+}$*;mef2c-AHF-Cre+;Rosa*$^{tdTom/+}$ (*VEGFR2*$^{SHF\text{-}Het}$) embryos. *VEGFR2*$^{+/-}$*;mef2c-AHF-Cre* mice were also crossed

135 with *Rosa*$^{tdTom/tdTom}$ mice to generate *VEGFR2*$^{+/+}$*;mef2c-AHF-Cre+;Rosa*$^{tdTom/+}$ (*VEGFR2*$^{SHF-WT}$)
136 embryos. To verify the ablation of VEGFR2 in the *mef2c-AHF*-lineage, we performed WM-IF and
137 used antibodies against VEGFR2 and tdTomato, encoded by the Cre-Reporter. In *VEGFR2*$^{SHF-}$
138 ^{WT} embryos, Cre-reporter+ cells in the anterior and posterior poles of the dorsal pericardial wall
139 and pharyngeal arches expressed VEGFR2 (**Fig. 1A-I**). In *VEGFR2*$^{SHF-KO}$ embryos, VEGFR2
140 expression was absent in the dorsal pericardial wall (**Fig. 1J-N, outlined**), and >80% of Cre-
141 reporter+ cells in the pharyngeal arches did not express VEGFR2 (**Figs. 1O-R arrows, Table**
142 **S2**). These experiments demonstrated the successful ablation of VEGFR2 protein from the
143 *mef2c-AHF*-lineage in *VEGFR2*$^{SHF-KO}$ embryos.

144 To determine whether the expression of VEGFR2 in the *mef2c-AHF*-lineage was required for PAA
145 development, we examined the formation of the PAAs in *VEGFR2*$^{SHF-WT}$, *VEGFR2*$^{SHF-Het}$ and
146 *VEGFR2*$^{SHF-KO}$ embryos at E10.5. Embryos were stained by WM-IF using antibodies against
147 VEGFR2, the ETS transcription factor ERG, and the Cre-reporter tdTomato. As with the *Isl1*$^{Cre/+}$
148 strain, we observed defective PAA formation in *VEGFR2*$^{SHF-Het}$ and *VEGFR2*$^{SHF-KO}$ embryos (**Fig.**
149 **2A-F, Table S1**). *VEGFR2*$^{SHF-Het}$ embryos had hypoplastic 6th PAAs (**Fig. 2C-D**). PAA defects in
150 *VEGFR2*$^{SHF-KO}$ mutants were more severe than in the *VEGFR2*$^{SHF-Het}$: both 4th and 6th PAAs were
151 mostly aplastic, with pharyngeal endothelium remaining in the primordial plexus form without
152 forming a central artery (**Fig. 2E-F**).

153 Quantitative analyses showed that the number of SHF-derived cells and the number of endothelial
154 cells were similar across all the genotypes (**Fig. 2G-H, Table S2-3**). However, the proportion of
155 pharyngeal arch ECs derived from the SHF was decreased in *VEGFR2*$^{SHF-Het}$ and *VEGFR2*$^{SHF-KO}$
156 embryos (**Fig. 2I, Table S3**). This indicates that VEGFR2 is not required for the presence of SHF-
157 derived cells in the pharyngeal arch mesenchyme but is necessary for their differentiation into
158 ECs. Since we observed similar phenotypes when ablating VEGFR2 using either the *Isl1*^{Cre} or
159 *mef2c-AHF-Cre* strains, these experiments indicate that the expression of *VEGFR2* in the SHF,
160 the common expression domain of the Cre recombinase in these strains, regulates the
161 differentiation of vascular progenitors.

162 Compared with controls, the proportion of SHF-derived ECs in *VEGFR2*$^{SHF-Het}$ was reduced about
163 2-fold in all pharyngeal arches (**Fig. 2I, Table S3**). These data indicate that the expression of one
164 copy of VEGFR2 was not sufficient for SHF-derived cells to adopt EC fate. In *VEGFR2*$^{SHF-KO}$, the
165 majority of pharyngeal arch ECs were not derived from the *mef2c-AHF* lineage; the proportions
166 of SHF-derived ECs were decreased by 3-, 10-, and 20-fold relative to controls in the 3rd, 4th, and

167 6th pharyngeal arches, respectively **(Fig. 2I, Table S3**). Together, these results reveal that an
168 alternative vascular source compensates for the reduction in SHF-derived ECs in *VEGFR2*$^{SHF\text{-}Het}$
169 and *VEGFR2*$^{SHF\text{-}KO}$ embryos and rescues the numbers of ECs in pharyngeal arches to control
170 levels.

171 **Compensatory endothelium rescues arch artery morphogenesis in *VEGFR2*$^{SHF\text{-}Het}$**
172 **embryos.**

173 Defective PAA formation leads to abnormal morphogenesis of the aortic arch and its branches
174 (Hutson and Kirby, 2007). To determine the role of SHF-derived endothelium in the remodeling
175 of PAAs into the aortic arch arteries (AAA), we examined embryos heterozygous or null for
176 VEGFR2 in either the *mef2c-AHF-Cre* or *Isl1*^{Cre} lineages after E14.5, when the remodeling of the
177 AAAs is complete. A Mendelian distribution of each genotype was observed between E14.5 and
178 P0, indicating that loss of SHF-derived vascular progenitors does not cause prenatal lethality
179 (**Table S4**). To identify defects in AAA development, embryos were analyzed at either E14.5 or
180 E18.5 by micro-computed tomography or conventional histology and H&E staining. 80% of
181 embryos null for VEGFR2 in the SHF from either the *Isl1*^{Cre} or *mef2c-AHF-Cre* lines developed
182 AAA defects (**Fig. 3; Table S5**). Despite a significantly decreased number of SHF-derived ECs in
183 the PAAs, only 1 out of 18 (5.6%) embryos heterozygous for VEGFR2 in the SHF had aberrant
184 AAA patterning, displaying RERSA (**Fig. 3A, Fig. S2, Table S6**). The AAA defects observed in
185 80% of conditional VEGFR2-null and 5.6% of conditional VEGFR2-heterozygous embryos
186 (**Tables S5-6**) were due to defective development and remodeling of the 4th PAAs (Stoller and
187 Epstein, 2005). This indicates that relative to the vessels arising from the 3rd and 6th PAAs, the
188 development of 4th PAA-derived vessels is more sensitive to the decrease in the numbers of SHF-
189 derived ECs.

190 Although *VEGFR2*$^{SHF\text{-}Het}$ and *VEGFR2*$^{SHF\text{-}KO}$ embryos had similar total numbers of ECs in each
191 pharyngeal arch (**Fig. 2H**), *VEGFR2*$^{SHF\text{-}KO}$ embryos displayed more severe defects in PAA
192 formation and subsequent AAA remodeling (**Fig. 3A, Table S5-6**). A notable difference between
193 these genotypic classes is the significant decrease in the proportion of SHF-derived cells in the
194 pharyngeal arches of *VEGFR2*$^{SHF\text{-}KO}$ embryos (**Fig. 2I, black bars**). These findings indicate that
195 SHF-derived ECs play a crucial role in PAA development and that a threshold number of SHF-
196 derived ECs is necessary for proper AAA morphogenesis.

197 ***Tbx1* regulates the recruitment of compensatory endothelium and the rescue of PAA**
198 **development.**

199 Fourth PAA-derived defects, such as IAA-B, are observed in about 19% of patients with 22q11DS
200 (Momma, 2010; Yagi et al., 2003). These patients have one functional copy of the *Tbx1* gene.
201 Meta-analyses of studies on different $Tbx1^{+/-}$ strains and df(16)1/+ mice, which model 22q11DS,
202 indicate that *Tbx1* heterozygosity results in defects in 4th PAA formation with an average
203 penetrance of 43% and defects in AAA development with an average penetrance of 36% (**Table**
204 **S7 – 8**) (Aggarwal et al., 2006; Calmont et al., 2009; Guris et al., 2006; Hasten and Morrow, 2019;
205 Jerome and Papaioannou, 2001; Lindsay et al., 1999; Lindsay and Baldini, 2001; Lindsay et al.,
206 2001; Merscher et al., 2001; Papangeli and Scambler, 2013; Phillips et al., 2019; Randall et al.,
207 2009; Ryckebusch et al., 2010; Stothard et al., 2020; Taddei et al., 2001; Vitelli et al., 2002; Zhang
208 and Baldini, 2008).

209 To investigate the role of *Tbx1* in PAA development and in the contribution of SHF-derived
210 progenitors to the PAA endothelium, we crossed $Tbx1^{+/-}$*;mef2c-AHF-Cre* mice with $Rosa^{tdTom/tdTom}$
211 mice. $Tbx1^{+/-}$ ($Tbx1^{+/-}$*;mef2c-AHF-Cre)* and control (*mef2c-AHF-Cre*) embryos were collected at
212 E10.5, and the total EC number and the number of SHF-derived ECs were quantified in the 4th
213 pharyngeal arches. We found that the 4th PAAs in $Tbx1^{+/-}$ embryos were either hypoplastic or
214 aplastic (**Fig. 4A-B, Table S1**). Quantitative analyses of EC populations indicated that unlike in
215 $VEGFR2^{SHF\text{-}Het}$ embryos, the total number of ECs in the 4th pharyngeal arches of $Tbx1^{+/-}$ mice was
216 reduced by 30% relative to controls ($p < 0.0001$, **Fig. 4C**). Our analyses of EC numbers indicated
217 that the average number of total ECs in the 4th pharyngeal arch was constant across five different
218 control genotypes examined in our lab in the past decade and is independent of the investigator
219 performing the analyses (**Fig. S3**) (Warkala et al., 2021). We also found that a 25-30% decrease
220 in the total number of ECs in the 4th pharyngeal arch, as seen in $Tbx1^{+/-}$ mice, leads to defective
221 formation of the 4th PAAs, resulting in IAA-B or RERSA (Warkala et al., 2021). Together, these
222 data are consistent with the idea that the ~476+/-81 ECs is the optimum EC number required for
223 the robust formation and remodeling of the 4th PAAs.

224 Although the number of SHF-derived ECs was similar between $Tbx1^{+/-}$ and $VEGFR2^{SHF\text{-}Het}$
225 embryos (**Fig. 4D**), the decrease in the SHF-derived EC population in $VEGFR2^{SHF\text{-}Het}$ was
226 complemented by the increase in the number of non-SHF derived ECs (**Fig. 4E, Table S3**). In
227 contrast, no such increase in non-SHF-derived ECs was observed in $Tbx1^{+/-}$ embryos (**Fig. 4E**).

228 Despite having a comparable number of SHF-derived ECs between *Tbx1*$^{+/-}$ and *VEGFR2*$^{SHF\text{-}Het}$
229 embryos, *Tbx1*$^{+/-}$ embryos develop AAA defects at a much higher penetrance (36% on average,
230 **Table S8**). These data indicate the recruitment of compensatory ECs rescues PAA and AAA
231 morphogenesis in *VEGFR2*$^{SHF\text{-}Het}$ embryos (**Tables S1** and **S6**). Therefore, it is crucial to
232 understand the source(s) of the compensatory ECs and the mechanisms that regulate their
233 recruitment.

234 **Ectopic sprouts in the pharyngeal region of *VEGFR2*$^{SHF\text{-}KO}$ embryos are absent in *Tbx1*$^{+/-}$**
235 **embryos.**

236 To determine the origin of compensatory endothelium in *VEGFR2*$^{SHF\text{-}KO}$ embryos, we analyzed
237 the 3D connectivity of vessels surrounding the pharyngeal arches in confocal images of E9.5
238 *VEGFR2*$^{SHF\text{-}WT}$ and *VEGFR2*$^{SHF\text{-}KO}$ embryos (27 – 29s). Located laterally to the PAAs is a network
239 of venous vasculature, including the cardinal vein (CV) and pharyngeal vein (PV, also known as
240 the ventral vein) (**Fig. 5A**). In contrast to the *VEGFR2*$^{SHF\text{-}WT}$ embryos (**Fig. 5B**), we observed
241 ectopic vascular sprouts from CV and PV connecting with the pharyngeal arch endothelium in
242 *VEGFR2*$^{SHF\text{-}KO}$ embryos, indicating a possible source of compensatory ECs (**Fig. 5C, yellow**
243 **bracket, and arrows**). These aberrant vascular connections were absent in *Tbx1*$^{+/-}$ embryos,
244 supporting the role of *Tbx1* in the recruitment of the rescuing endothelium (**Fig. 5D, red**
245 **asterisks**).

246 **Angiogenic sprouting from veins gives rise to the compensatory endothelium rescuing**
247 **PAA morphogenesis.**

248 To investigate whether non-SHF-derived ECs in *VEGFR2*$^{SHF\text{-}KO}$ pharyngeal arches originate from
249 the surrounding veins, we used lineage tracing to label venous endothelium in *VEGFR2*$^{SHF\text{-}KO}$
250 embryos. First, we employed the *ApjCreERT2* transgenic strain (Chen et al., 2014) and tamoxifen
251 to induce Cre-mediated recombination at E9.5 and observed extensive labeling of venous
252 vasculature, including the PV, CV, and venous intersomitic branches in wild-type embryos (**Fig.**
253 **S4A**); arterial structures, including the dorsal aorta, arterial intersomitic branches, and PAAs were
254 not labeled except for one or two cells (**Fig. S4B**), indicating specificity for venous lineage tracing.
255 To label venous vasculature in *VEGFR2*$^{SHF\text{-}KO}$ embryos, we generated the *Apj*$^{DreERT2/+}$ knock-in
256 strain and obtained *VEGFR2*$^{SHF\text{-}WT}$*;Apj*$^{DreERT2/+}$ or *VEGFR2*$^{SHF\text{-}KO}$*;Apj*$^{DreERT2/+}$ embryos. Lineage
257 tracing of the venous vasculature revealed a significant increase in *Apj*-derived ECs in the 4th PAA
258 of *VEGFR2*$^{SHF\text{-}KO}$ compared to *VEGFR2*$^{SHF\text{-}WT}$ embryos (**Fig. 6A-E**). Importantly, we did not

observe any labeling of the dorsal aorta or its angiogenic sprouts, indicating high specificity of venous lineage labeling (**Fig. 6B and D, white arrows**). Immunofluorescence staining and single-molecule (sm) RNA-FISH experiments confirmed an increase in the number of ECs expressing venous markers COUP-TFII and *Apj* in the 4th pharyngeal arches of *VEGFR2*$^{SHF\text{-}KO}$ embryos (**Fig. 6F-K)**. Our results indicate that angiogenesis from the venous endothelium generates compensatory ECs, restoring the total number of pharyngeal arch ECs in *VEGFR2*$^{SHF\text{-}KO}$ embryos to control levels.

Increased *VEGFA* mRNA expression drives ectopic angiogenesis from veins.

Next, we aimed to determine mechanisms regulating the recruitment of compensatory venous endothelium. We hypothesized that the loss of VEGFR2+ SHF-derived vascular progenitors in pharyngeal arches would result in increased expression of proangiogenic factors, such as VEGFA. To test this, we performed smRNA-FISH to examine *VEGFA* mRNA at early E9.5 before the 4th PAA forms. Quantification showed a significant increase of *VEGFA* mRNA levels in the SHF and pharyngeal endoderm of *VEGFR2*$^{SHF\text{-}KO}$ embryos, compared to *VEGFR2*$^{SHF\text{-}WT}$ (**Fig. 7**). These results suggest that the loss of VEGFR2 in the SHF and the consequent inability of SHF-derived ECs to contribute to the PAAs results in an increased expression of *VEGFA*, which in turn drives ectopic angiogenesis from the surrounding venous vasculature to rescue pharyngeal arch artery development.

Discussion

Proper development and remodeling of the PAAs, particularly the left 4th PAA, is crucial for establishing appropriate blood circulation after birth. Elucidating the mechanisms underlying arch artery formation and the response of the pharyngeal arch microenvironment to genetic perturbations is essential for understanding how genetic mutations lead to CHD phenotypes, such as IAA-B. Through our investigations, we have identified several critical factors that contribute to proper arch artery morphogenesis and uncovered a previously unknown ability of the developing mammalian embryo to restore and regenerate the PAA endothelium.

The phenomenon of development remaining relatively constant despite genetic and environmental disturbances has captivated and confounded researchers. In 1942, Waddington proposed the concept of buffering to explain this remarkable characteristic of multicellular organisms. He further hypothesized that this buffering capacity is based on an optimum and a

threshold stimuli, beyond which the optimal response can no longer be achieved (Waddington, 1942). However, despite a few notable studies (Abrams et al., 2015; Jelier et al., 2016; Sharma et al., 2017), our understanding of buffering processes and their underlying mechanisms still needs to be improved.

Our study uncovers a heretofore unknown capacity of the mammalian embryo to repair and regenerate the aortic arch artery development against genetic perturbations. Our findings suggest that there exists both a threshold and an optimum number of SHF-derived ECs needed for robust arch artery development. The expression of *VEGFR2* and *Tbx1* regulates this optimum number in a dosage-dependent manner. Our studies suggest that crosstalk between SHF-derived ECs and the surrounding pharyngeal tissues regulates the addition of compensating endothelium to the PAAs. In the presence of the optimal number of SHF-derived ECs, ectopic angiogenesis is suppressed. We hypothesize that there may be an evolutionary advantage for the formation of the PAAs from progenitors in the SHF. However, when the number of SHF-derived ECs falls below the optimum, the pharyngeal tissue microenvironment is modified, resulting in increased synthesis of *VEGFA*, eliciting an angiogenic response from the veins. 3D vessel tracing, gene expression, and lineage mapping indicate that the angiogenic response from the venous endothelium provides compensatory endothelium rebuilding the PAAs. Our studies also reveal the existence of a threshold number of SHF-derived ECs, below which arch artery development becomes unpredictable, as in *VEGFR2*$^{SHF\text{-}KO}$ embryos.

Most patients with 4th PAA-derived CHDs, including IAA-B, are diagnosed with 22q11DS (Moerman et al., 1987; Van Mierop and Kutsche, 1986a). Studies using *Tbx1*$^{+/-}$ mice have demonstrated that these defects are attributed to haploinsufficiency in the *Tbx1* gene. The expression of *Tbx1* in splanchnic mesoderm and pharyngeal epithelia is required for PAA development (Jerome and Papaioannou, 2001; Lindsay et al., 2001; Merscher et al., 2001; Zhang, 2006; Zhang et al., 2005). Our research shows that *Tbx1* is a critical regulator of the contribution of SHF-derived progenitors to the PAA endothelium and that the heterozygosity of *Tbx1* results in a penetrant phenotype consisting of aplastic and hypoplastic PAAs. Interestingly, the number of SHF-derived ECs in *Tbx1*$^{+/-}$ embryos is comparable to that in *VEGFR2*$^{SHF\text{-}Het}$ embryos; yet *Tbx1*$^{+/-}$ embryos lack the compensating endothelium and develop AAA defects with a penetrance of approximately 36% (**Table S8**). In contrast, the incidence of AAA defects in *VEGFR2*$^{SHF\text{-}Het}$ mice, where compensatory endothelium is recruited, is much lower at approximately 6%. Altogether, these studies indicate that the threshold number of SHF-derived endothelial cells is

321 insufficient to support proper PAA formation and aortic arch morphogenesis in the absence of the
322 compensatory endothelium.

323 Our studies suggest that the absence of compensatory endothelium in *Tbx1*$^{+/-}$ embryos impacts
324 the ability of aplastic PAAs to recover and properly remodel into the AAAs. Thus, *Tbx1* regulates
325 the buffering capacity during arch artery development in a dosage-dependent manner. Our
326 experiments show that *Tbx1* mediates the recruitment of the venous endothelium by regulating
327 angiogenic sprouting. Taken together, these findings uncover the buffering mechanism underlying
328 robustness and plasticity in the development of the aortic arch. Further understanding of how
329 *Tbx1* impacts the rescue of the PAA endothelium can lead to the prevention or treatment of CHD
330 phenotypes associated with 22q11DS.

331 **Methods:** Detailed methods are provided in a separate file

332 **Author contributions:** AJR and SA conceived and designed the experiments; AJR performed
333 all the experiments, KD processed embryos for microCT imaging, and helped with the analyses
334 and interpretation of congenital heart defects. AJR and SA analyzed the data and wrote the paper.

335 **Acknowledgments:** We thank Sam Russo and Bogdana Mimic for their technical assistance. Xia
336 Wang, for teaching all the experimental techniques. Caolán O'Donnell, Brianna Alexander, Cecilia
337 Arriagada, Gideon Obeng, Michael Warkala, and Huaning Zhao for reading the paper and for their
338 helpful suggestions throughout this work. Brittany Ramirez for her artistic expertise. This work
339 was supported by funding from the National Heart, Lung, and Blood Institute of the National
340 Institutes of Health grants R01 HL103920, R01 HL134935, and R01 HL158049, and a
341 Transformational Project Award from the American Heart Association 20TPA35490074 to S.A.
342 AJR was supported by National Heart, Lung, and Blood Institute of the National Institutes of Health
343 pre-doctoral fellowships F31 HL150949, HL103920-08S1, and by the National Institute of Arthritis
344 and Musculoskeletal and Skin Diseases training grant T32052273-11.

345 **Figure Legends**

346 **Main Figures**

347 **Figure 1. Efficient ablation of VEGFR2 in the second heart field (SHF) using *mef2c-AHF-***
348 ***Cre* mice.** Cre-lox recombination and immunofluorescent staining were used to trace *mef2c-AHF-*
349 *Cre* lineage cells (cyan) when VEGFR2 (magenta) is conditionally ablated from the SHF in

350 embryos. **(A-E)** Optical confocal sections of E9.5 *VEGFR2*$^{SHF\text{-}WT}$ embryos show VEGFR2+ cells
351 in the anterior **(B-C)** and posterior **(D-E)** dorsal pericardial wall outlined in yellow. **(F-I)** PAA ECs
352 in E10.5 *VEGFR2*$^{SHF\text{-}WT}$ embryos are derived from the SHF. The box in F is expanded in **(G-I)**.
353 Arrowheads point to the co-expression of VEGFR2 (magenta), ERG (orange), and Cre-reporter
354 (cyan) in the 4th pharyngeal arch endothelium. **(J-N)** Optical sections of E9.5 *VEGFR2*$^{SHF\text{-}KO}$
355 embryos show the absence of VEGFR2 expression in the anterior **(K-L)** and posterior SHF dorsal
356 pericardial wall **(M-N),** outlined in yellow. **(O-R)** PAA ECs in E10.5 *VEGFR2*$^{SHF\text{-}KO}$ embryos are
357 derived from a non-SHF endothelium. The box in **O** is expanded in **(P-R).** Arrowheads point to
358 Cre-reporter negative endothelium. Arrows point to Cre-reporter+ VEGFR2-negative cells.

359 **Figure 2. VEGFR2 is required for SHF vascular progenitor contribution and PAA**
360 **development.**

361 **(A-F)** WM-IF for VEGFR2 (magenta) and Cre-reporter (cyan), confocal imaging, and 3D
362 reconstruction of E10.5 **(A)** *VEGFR2*$^{SHF\text{-}WT}$, **(C)** *VEGFR2*$^{SHF\text{-}Het}$, and **(E)** *VEGFR2*$^{SHF\text{-}KO}$ embryos.
363 Yellow brackets highlight aberrant PAAs in **C, E**. Dashed lines mark the levels of coronal optical
364 sections through the pharyngeal arches shown in **B, D,** and **F**. Dotted circles mark aberrant PAAs.
365 **(G)** Quantification of SHF-derived cells in each pharyngeal arch. *VEGFR2*$^{SHF\text{-}WT}$ n = 10 arches,
366 *VEGFR2*$^{SHF\text{-}Het}$ n = 4 arches, *VEGFR2*$^{SHF\text{-}KO}$ n = 6 arches. Each dot marks one pharyngeal arch.
367 Horizontal red and black lines mark means and quartiles, respectively. **(H)** Quantification of total
368 EC numbers in each pharyngeal arch. *VEGFR2*$^{SHF\text{-}WT}$ n = 10 arches, *VEGFR2*$^{SHF\text{-}Het}$ n = 12 arches,
369 *VEGFR2*$^{SHF\text{-}KO}$ n = 12 arches. Each dot marks one pharyngeal arch. Horizontal red and black lines
370 mark means and quartiles, respectively. **(I)** The proportion of Cre-reporter-positive ECs and Cre-
371 reporter-negative ECs in each pharyngeal arch. Means ± SD are shown. *VEGFR2*$^{SHF\text{-}WT}$ n = 10
372 arches, *VEGFR2*$^{SHF\text{-}Het}$ n = 12 arches, *VEGFR2*$^{SHF\text{-}KO}$ n = 12 arches. Data were analyzed using
373 two-way ANOVA with Tukey's correction for multiple testing; *$p \leq 0.05$ **$p \leq 0.01$, ***$p \leq 0.001$,
374 ****$p < 0.0001$

375 **Figure 3. A threshold number of SHF-derived ECs is required for proper Aortic Arch Artery**
376 **development.**

377 **(A)** Percent of *VEGFR2;Isl1*^{Cre} (*VEGFR2*$^{Isl1\text{-}WT}$, *VEGFR2* $^{Isl1\text{-}Het}$, and *VEGFR2* $^{Isl1\text{-}KO}$) and -
378 *VEGFR2;mef2c-AHF-Cre* (*VEGFR2*$^{SHF\text{-}WT}$, *VEGFR2*$^{SHF\text{-}Het}$, and *VEGFR2*$^{SHF\text{-}KO}$) embryos without
379 AAA defects (white), non-lethal AAA defects (grey), or lethal AAA defects (black). n = the number
380 of embryos with each phenotype. **(B-D)** Transverse sections of E18.5 embryos stained with

381 Hematoxylin and eosin. **(B)** *VEGFR2*$^{SHF\text{-}WT}$ embryos. **(C)** IAAB and **(D)** RERSA in *VEGFR2*$^{Isl1\text{-}KO}$
382 and *VEGFR2*$^{SHF\text{-}KO}$ embryos, respectively. **(E-G)** Micro-computed tomography of E18.5
383 *VEGFR2*$^{Isl1\text{-}WT}$ **(E)** and *VEGFR2*$^{Isl1\text{-}KO}$ **(F-G)** embryos. Arrows and text indicate examples of IAAB
384 **(F)** and aberrant RScA **(G)** in yellow. Dotted boxes highlight the position of a normal aortic arch.
385 **Abbreviations:** RCA – right carotid artery; LCA – left carotid artery; RScA – right subclavian
386 artery; LScA – left subclavian artery; BrA – brachiocephalic artery; AoA – aortic arch; PT –
387 pulmonary trunk; DA – ductus arteriosus; dAo – descending aorta; TR – trachea; IAA-B –
388 interrupted aortic arch type B; RERSA – retroesophageal right subclavian artery

389 **Figure 4. *Tbx1* regulates endothelial compensation and rescue of PAA development.**

390 **(A-B)** WM-IF for VEGFR2 (magenta) and Cre-reporter (cyan) of an E10.5 *Tbx1*$^{+/-}$ embryo. **(A)** 3D
391 reconstruction and **(B)** coronal optical sections show the incomplete formation of the 4th PAA
392 (dotted circles) and that only a few non-SHF-derived ECs are present. **(C)** Quantification of ECs
393 in the 4th pharyngeal arches of control (*mef2c-AHF-Cre*), *Tbx1*$^{+/-}$, and *VEGFR2*$^{SHF\text{-}Het}$ embryos.
394 Each dot marks one pharyngeal arch. Horizontal red and black lines mark means and quartiles,
395 respectively. **(D)** Quantification of the number of SHF-derived (Cre-reporter positive) ECs in the
396 4th pharyngeal arch. Error bars represent mean ± SD. **(E)** Quantification of the number of non-
397 SHF-derived (Cre-reporter negative) ECs in the 4th pharyngeal arch. Error bars represent mean
398 ± SD. Control n = 14 arches, *Tbx1*$^{+/-}$*;mef2c-AHF-Cre* n = 6 arches, SHF-het n = 12 arches. Data
399 were analyzed using one-way ANOVA with Tukey's correction for multiple testing; **$p \leq 0.01$,
400 ****$p < 0.0001$

401 **Figure 5. Ectopic sprouts from veins in the pharyngeal region of *VEGFR2*$^{SHF\text{-}KO}$ are absent**
402 **in *Tbx1*$^{+/-}$ embryos**

403 **(A)** A schematic depiction of venous and arterial vasculature in the pharyngeal region of E9.5
404 embryos. dAo – dorsal aorta; CV – cardinal vein; PV – pharyngeal vein. **(B-D)** 20μm-thick serial
405 sagittal optical sections through E9.5 *VEGFR2*$^{SHF\text{-}WT}$ **(B)**, *VEGFR2*$^{SHF\text{-}KO}$ **(C)**, and *Tbx1*$^{+/-}$ **(D)**
406 embryos from the lateral to the medial side. Yellow brackets in B-D mark pharyngeal endothelial
407 plexus. Red stars mark absent venous sprouts in *VEGFR2*$^{SHF\text{-}WT}$ **(B)** and *Tbx1*$^{+/-}$ **(D)** embryos.
408 Yellow, magenta, and cyan arrows follow sprouts from the CV to the pharyngeal arch vasculature
409 in the *VEGFR2*$^{SHF\text{-}KO}$ embryos **(C)**.

410 **Figure 6. Angiogenic sprouting from veins gives rise to the compensatory endothelium**
411 **that rescues PAA morphogenesis.**

412 Dre-rox recombination was used to fate map cells of Apj-lineage in *VEGFR2*$^{SHF\text{-}KO}$ and
413 *VEGFR2*$^{SHF\text{-}WT}$ embryos. Tamoxifen was injected at E9.5, and embryos were dissected at E10.5.
414 **(A-D)** WM-IF staining detecting Dre-reporter (cyan) and VEGFR2 (magenta). 50μm-thick sagittal
415 optical sections show *Apj*^{DreERT2} lineage labeling in the CV and intersomitic veins (yellow arrows)
416 but not the dAo or intersomitic arteries (white arrows) of **(A)** *VEGFR2*$^{SHF\text{-}WT}$ and **(C)** *VEGFR2*$^{SHF\text{-}}$
417 ^{KO} embryos. Boxes in **B, D** are expanded in the panels on the right to show *Apj*^{DreERT2} lineage
418 labeled ECs in the 4th PAAs of *VEGFR2*$^{SHF\text{-}KO}$ embryos **(**arrowheads, **D)** but not in control,
419 *VEGFR2*$^{SHF\text{-}WT}$ embryos **(B)**. **(E)** *VEGFR2*$^{SHF\text{-}KO}$ embryos have a higher percent contribution of
420 Apj-lineage cells in the 4th PAAs. The number of Apj-lineage cells in arches was normalized by
421 *Apj*^{DreERT2} labeling efficiency (see Methods and **Fig. S4C-D**). Each dot marks one pharyngeal arch.
422 Horizontal red and black lines mark means and quartiles, respectively. Control n = 10 arches,
423 mutant n = 6 arches. **(F-G)** WM-IF for COUPTF2 (magenta) and VEGFR2 (white) of E9.5
424 embryos. 20μm-thick sagittal optical sections: **F.** *VEGFR2*$^{SHF\text{-}WT}$ and **G.** *VEGFR2*$^{SHF\text{-}KO}$ embryos.
425 Yellow arrows point to COUPTF2+ ECs in the CV. White arrows point to COUPTF2-negative ECs
426 in 3rd PAA and dAo. Arrowheads point to COUPTF2+ ECs in the 4th PAA of *VEGFR2*$^{SHF\text{-}KO}$ embryo
427 (**G**). **(H)** Quantification of COUPTF2+ ECs in the 4th pharyngeal arches. Each dot marks one
428 pharyngeal arch. Horizontal red and black lines mark means and quartiles, respectively. Control
429 n = 9 arches, mutant n = 7 arches. **(I-J)** Confocal optical sections. Single-molecule RNA
430 fluorescence *in situ* hybridization for *Apj* mRNA (magenta) combined with immunostaining for
431 VEGFR2 (white) of E10.0 embryos. Yellow arrows point to *Apj*+ ECs in the CV. White arrows
432 point to Apj-negative ECs in 3rd PAA and dAo. **(K)** Quantification of *Apj*+ ECs in the 4th pharyngeal
433 arches. Each dot marks one pharyngeal arch. Horizontal red and black lines mark means and
434 quartiles, respectively. Control n = 6 arches, mutant n = 7 arches. Data were analyzed using 2-
435 tailed, unpaired Student's t-test; *$p \leq 0.05$, ** $p \leq 0.01$, ***$p \leq 0.001$.

436 **Figure 7. Loss of SHF-derived vascular progenitors increases *VEGFA* mRNA expression**
437 **in the SHF and pharyngeal endoderm.**

438 **(A-B)** Single-molecule RNA fluorescent *in situ* hybridization of E9.5 embryos detecting the
439 expression of *VEGFA* (white) in the SHF (outlined in red) and pharyngeal endoderm (outlined in
440 yellow). **(C)** Super plot of normalized mean fluorescence intensity of *VEGFA* mRNA in the SHF.
441 **(D)** Super plot of normalized mean fluorescence intensity of *VEGFA* mRNA in the pharyngeal

endoderm. The mean fluorescence intensity in the SHF and pharyngeal endoderm was normalized to the mean fluorescence intensity in the dorsal side of the embryo on the same optical section (outlined in green). Different colors in **C, D** mark different biological samples. Light-colored dots mark individual measurements in optical sections. Dark-colored dots mark the average of measurements per pharyngeal arch. Red lines mark means, and black lines mark quartiles**.** Control n = 6 arches, mutant n = 6 arches. Data were analyzed using 2-tailed, unpaired Student's t-test; **$p \leq 0.01$.

Supplemental Figures

Supplemental Figure 1. VEGFR2 is required in the *Isl1*-lineage for PAA development.

(A-F) WM-IF to detect VEGFR2 (magenta), confocal imaging, and 3D reconstruction of **(A)** *VEGFR2*$^{Isl1\text{-}WT}$, **(C)** *VEGFR2*$^{Isl1\text{-}Het}$, and **(E)** *VEGFR2*$^{Isl1\text{-}KO}$ embryos isolated at E10.5. Dashed lines mark levels of coronal optical sections shown in **B, D, F**. Yellow bracket highlights aberrant PAAs in **E**. Dotted circles mark aberrant PAAs in **D, F**. **G – I.** WM-IF on E10.5 embryos to detect VEGFR2 (magenta) and lineage (cyan). Dotted line outlines the dorsal pericardial wall. Genotypes are marked at the top, and somite (s) stages are included in each panel.

Supplemental Figure 2.

(A) Transverse sections of E18.5 *VEGFR2*$^{SHF\text{-}Het}$ embryo showing RERSA (arrow) stained with hematoxylin and eosin.

Supplemental Figure 3.

(A) Meta-analysis of total 4th pharyngeal arch EC numbers across five control genotypes: *VEGFR2*$^{+/+}$*;mef2c-AHF-Cre*, *Tbx1*$^{+/-}$*;mef2c-AHF-Cre* (this manuscript), *α5*$^{f/+}$*;Isl1*$^{Cre/+}$; *Fn1*$^{f/+}$*;Isl1*$^{Cre/+}$ and wild-type (*C57BL6/J*) (analyses in Warkala et al., 2021 were performed by three different investigators independently over course of eight years). Red lines mark means, and black lines mark quartiles. Data were analyzed using a 2-tailed, unpaired Student's t-test; $p>0.05$ was considered not significant.

Supplemental Figure 4.

468 **(A-B)** WM-IF staining detecting Cre-reporter (cyan) and VEGFR2 (magenta). 50μm-thick sagittal
469 optical sections show *ApjCreERT2* lineage labeling in the CV and intersomitic veins (yellow
470 arrows) but not the dAo or intersomitic arteries (white arrows). Few Cre-reporter cells can be seen
471 in the PAA endothelium. PAAs are numbered. **(C)** WM-IF staining detecting Dre-reporter (cyan),
472 ERG (magenta), and VEGFR2 (grey). 100μm-thick sagittal optical section shows the region of the
473 CV used to calculate Dre-recombination efficiency (outlined in yellow) in $Apj^{DreERT2}$ embryos. **(D)**
474 Comparable Dre-recombination efficiency in $VEGFR2^{SHF\text{-}WT}$; $Apj^{DreERT2}$ and $VEGFR2^{SHF\text{-}KO}$;
475 $Apj^{DreERT2}$ embryos at E10.5. Data were analyzed using 2-tailed, unpaired Student's t-test; $p>0.05$
476 was considered not significant.

477 **Supplemental Tables**

478 **Supplemental Table 1. Penetrance of aberrant PAA formation.** PAAs of E10.5 embryos
479 ranging from 34-36s were analyzed via WM-IF staining for VEGFR2. Aberrant PAAs were marked
480 as "hypoplastic" when their diameter was markedly smaller than controls or as "aplastic,"
481 indicating the absence of a PAA (e.g., **Fig. 2** and **Fig. S1**). "0" indicates PAAs comparable to
482 controls. n = the number of individual pharyngeal arches analyzed. Percent of penetrance is
483 reported in paratheses.

484 **Supplemental Table 2. The average number of SHF-derived ECs in the pharyngeal arches.**
485 PAAs of E10.5 $VEGFR2^{SHF\text{-}WT}$ and $VEGFR2^{SHF\text{-}KO}$ embryos ranging from 34-36s were analyzed
486 via WM-IF staining. The total number of SHF cells was quantified in each pharyngeal arch.
487 Percent of VEGFR2-positive and VEGFR2-negative SHF cells was quantified. Averages ± SD are
488 reported in the table. Statistical analyses were reported in **Fig. 2G**.

489 **Supplemental Table 3. The average number ECs in the pharyngeal arches.** PAAs of E10.5
490 $VEGFR2^{SHF\text{-}WT}$, $VEGFR2^{SHF\text{-}Het}$, $VEGFR2^{SHF\text{-}KO}$, and $Tbx1^{+/-}$ embryos ranging from 34-36s were
491 analyzed via WM-IF. The total number of EC cells was quantified per pharyngeal arch. Percent
492 of SHF-derived and non-SHF-derived ECs was quantified. Averages ± SD are reported in the
493 table. Statistical analyses were reported in **Fig. 2H-I**.

494 **Supplemental Table 4. Loss of VEGFR2 in the SHF is not embryonic lethal.** Observed and
495 expected values of embryos dissected between E14.5 and P0 for each genotype. n = the number
496 of embryos observed and expected. Percent of each is reported in paratheses. Statistics were
497 evaluated using Chi-squared test.

498 **Supplemental Table 5. Cardiovascular defects in *VEGFR2*$^{Isl1\text{-}KO}$ and *VEGFR2*$^{SHF\text{-}KO}$ embryos.**
499 **Abbreviations**: H&E – hematoxylin and eosin; µCT – micro-computed tomography; RScA – right
500 subclavian artery; IAA-B – interrupted aortic arch type B; IAA-C – interrupted aortic arch type C.
501 Arch artery defects lethal postnatally are labeled in red and marked by an asterisk.

502 **Supplemental Table 6. Cardiovascular defects in *VEGFR2*$^{Isl1\text{-}Het}$ and *VEGFR2*$^{SHF\text{-}Het}$ embryos.**
503 **Abbreviations**: H&E – hematoxylin and eosin; µCT – micro-computed tomography; RScA – right
504 subclavian artery.

505 **Supplemental Table 7. Meta-analyses of PAA defects in 22Q11DS models**

506 **Supplemental Table 8. Meta-analyses of AAA defects in 22Q11DS models**

507

508 **References**

509 Abrams, M.J., Basinger, T., Yuan, W., Guo, C.L., Goentoro, L., 2015. Self-repairing symmetry in
510 jellyfish through mechanically driven reorganization. Proc Natl Acad Sci U S A 112, E3365-
511 3373.

512 Aggarwal, V.S., Liao, J., Bondarev, A., Schimmang, T., Lewandoski, M., Locker, J., Shanske,
513 A., Campione, M., Morrow, B.E., 2006. Dissection of Tbx1 and Fgf interactions in mouse models
514 of 22q11DS suggests functional redundancy. Hum Mol Genet 15, 3219-3228.

515 Anderson, R.H., Bamforth, S.D., 2022. Morphogenesis of the Mammalian Aortic Arch Arteries.
516 Front Cell Dev Biol 10, 892900.

517 Benjamin, E.J., Virani, S.S., Callaway, C.W., Chamberlain, A.M., Chang, A.R., Cheng, S.,
518 Chiuve, S.E., Cushman, M., Delling, F.N., Deo, R., de Ferranti, S.D., Ferguson, J.F., Fornage,
519 M., Gillespie, C., Isasi, C.R., Jiménez, M.C., Jordan, L.C., Judd, S.E., Lackland, D., Lichtman,
520 J.H., Lisabeth, L., Liu, S., Longenecker, C.T., Lutsey, P.L., Mackey, J.S., Matchar, D.B.,
521 Matsushita, K., Mussolino, M.E., Nasir, K., O'Flaherty, M., Palaniappan, L.P., Pandey, A.,
522 Pandey, D.K., Reeves, M.J., Ritchey, M.D., Rodriguez, C.J., Roth, G.A., Rosamond, W.D.,
523 Sampson, U.K.A.A., Satou, G.M., Shah, S.H., Spartano, N.L., Tirschwell, D.L., Tsao, C.W.,
524 Voeks, J.H., Willey, J.Z., Wilkins, J.T., Wu, J.H.Y., Alger, H.M., Wong, S.S., Muntner, P., 2018.
525 Heart Disease and Stroke Statistics—2018 Update: A Report From the American Heart
526 Association, Circulation, pp. e67-e492.

527 Calmont, A., Ivins, S., Van Bueren, K.L., Papangeli, I., Kyriakopoulou, V., Andrews, W.D.,
528 Martin, J.F., Moon, A.M., Illingworth, E.A., Basson, M.A., Scambler, P.J., 2009. Tbx1 controls
529 cardiac neural crest cell migration during arch artery development by regulating Gbx2
530 expression in the pharyngeal ectoderm, Development, pp. 3173-3183.

531 Celoria, G., Patton, R., 1959. Congenital absence of the aortic arch. American Heart Journal 58,
532 407-413.

533 Chen, H.I., Sharma, B., Akerberg, B.N., Numi, H.J., Kivela, R., Saharinen, P., Aghajanian, H.,
534 McKay, A.S., Bogard, P.E., Chang, A.H., Jacobs, A.H., Epstein, J.A., Stankunas, K., Alitalo, K.,
535 Red-Horse, K., 2014. The sinus venosus contributes to coronary vasculature through VEGFC-
536 stimulated angiogenesis, Development, pp. 4500-4512.

537 Collins-Nakai, R.L., Dick, M., Parisi-Buckley, L., Fyler, D.C., Castaneda, A.R., 1976. Interrupted
538 aortic arch in infancy. The Journal of Pediatrics 88, 959-962.

539 Goldmuntz, E., Driscol, D.A., Budarf, M.L., Zackai, E., McDonald-McGinn, D.M., Biegel, J.A.,
540 Emanuel, B.S., 1993. Microdeletions of chromosomal region 22q11 in patients with congenital
541 conotruncal cardiac defects. Journal of medical genetics 30, 807-812.

542 Graham, A., 2003. Development of the pharyngeal arches. Am J Med Genet A 119A, 251-256.

543 Guris, D.L., Duester, G., Papaioannou, V.E., Imamoto, A., 2006. Dose-dependent interaction of
544 Tbx1 and Crkl and locally aberrant RA signaling in a model of del22q11 syndrome. Dev Cell 10,
545 81-92.

546 Hasten, E., Morrow, B.E., 2019. Tbx1 and Foxi3 genetically interact in the pharyngeal pouch
547 endoderm in a mouse model for 22q11.2 deletion syndrome. PLoS Genet 15, e1008301.

548 Hutson, M.R., Kirby, M.L., 2007. Model systems for the study of heart development and disease
549 Cardiac neural crest and conotruncal malformations, Seminars in Cell & Developmental Biology,
550 pp. 101-110.

551 Jelier, R., Kruger, A., Swoger, J., Zimmermann, T., Lehner, B., 2016. Compensatory Cell
552 Movements Confer Robustness to Mechanical Deformation during Embryonic Development.
553 Cell Syst 3, 160-171.

554 Jerome, L.A., Papaioannou, V.E., 2001. DiGeorge syndrome phenotype in mice mutant for the
555 T-box gene, Tbx1, Nature Genetics, pp. 286-291.

556 Kau, T., Sinzig, M., Gasser, J., Lesnik, G., Rabitsch, E., Celedin, S., Eicher, W., Illiasch, H.,
557 Hausegger, K., 2007. Aortic Development and Anomalies, Seminars in Interventional Radiology,
558 pp. 141-152.

559 Levitt, B., Richter, J.E., 2007. Dysphagia lusoria: a comprehensive review. Dis Esophagus 20,
560 455-460.

561 Li, P., Pashmforoush, M., Sucov, H.M., 2012. Mesodermal retinoic acid signaling regulates
562 endothelial cell coalescence in caudal pharyngeal arch artery vasculogenesis. Dev Biol 361,
563 116-124.

564 Lindsay, E., Botta, A., Vesna, J., Carattini-Rivera, S., Cheah, Y.-C., Rosenblatt, H.M., Bradley,
565 A., Baldini, A., 1999. Congenital heart disease in mice deficient for the DiGeorge syndrome
566 region. Nature 401, 379-383.

567 Lindsay, E.A., Baldini, A., 2001. Recovery from arterial growth delay reduces penetrance of
568 cardiovascular defects in mice deleted for the DiGeorge syndrome region. Human Molecular
569 Genetics 10, 997-1002.

570 Lindsay, E.a., Vitelli, F., Su, H., Morishima, M., Huynh, T., Pramparo, T., Jurecic, V., Ogunrinu,
571 G., Sutherland, H.F., Scambler, P.J., Bradley, a., Baldini, a., 2001. Tbx1 haploinsufficieny in the
572 DiGeorge syndrome region causes aortic arch defects in mice., Nature, pp. 97-101.

573 McDonald-McGinn, D.M., Sullivan, K.E., 2011. Chromosome 22q11.2 deletion syndrome
574 (DiGeorge syndrome/velocardiofacial syndrome). Medicine (Baltimore) 90, 1-18.

575 McDonald-McGinn, D.M., Sullivan, K.E., Marino, B., Philip, N., Swillen, A., Vorstman, J.A.,
576 Zackai, E.H., Emanuel, B.S., Vermeesch, J.R., Morrow, B.E., Scambler, P.J., Bassett, A.S.,
577 2015. 22q11.2 deletion syndrome. Nat Rev Dis Primers 1, 15071.

578 Merscher, S., Funke, B., Epstein, J.A., Heyer, J., Puech, A., Lu, M.M., Xavier, R.J., Demay,
579 M.B., Russell, R.G., Factor, S., Tokooya, K., Jore, B.S., Lopez, M., Pandita, R.K., Lia, M.,
580 Carrion, D., Xu, H., Schorle, H., Kobler, J.B., Scambler, P., Wynshaw-Boris, A., Skoultchi, A.I.,
581 Morrow, B.E., Kucherlapati, R., 2001. TBX1 is responsible for cardiovascular defects in velo-
582 cardio-facial/DiGeorge syndrome, Cell, pp. 619-629.

583 Moerman, P., Dumoulin, M., Lauweryns, J., Van der Hauwaert, L.G., 1987. Interrupted right
584 aortic arch in DiGeorge syndrome., Heart, pp. 274-278.

585 Momma, K., 2010. Cardiovascular anomalies associated with chromosome 22q11.2 deletion
586 syndrome. Am J Cardiol 105, 1617-1624.

587 Nagelberg, D., Wang, J., Su, R., Torres-Vázquez, J., Targoff, K.L., Poss, K.D., Knaut, H., 2015.
588 Origin, specification, and plasticity of the great vessels of the heart, Current Biology, pp. 2099-
589 2110.

590 Paffett-Lugassy, N., Singh, R., Nevis, K.R., Guner-Ataman, B., O'Loughlin, E., Jahangiri, L.,
591 Harvey, R.P., Burns, C.G., Burns, C.E., 2013. Heart field origin of great vessel precursors relies
592 on nkx2.5-mediated vasculogenesis, Nature Cell Biology, pp. 1362-1369.

593 Papangeli, I., Scambler, P.J., 2013. Tbx1 Genetically Interacts With the Transforming Growth
594 Factor- /Bone Morphogenetic Protein Inhibitor Smad7 During Great Vessel Remodeling,
595 Circulation Research, pp. 90-102.

596 Phillips, H.M., Stothard, C.A., Shaikh Qureshi, W.M., Kousa, A.I., Briones-Leon, J.A.,
597 Khasawneh, R.R., O'Loughlin, C., Sanders, R., Mazzotta, S., Dodds, R., Seidel, K., Bates, T.,
598 Nakatomi, M., Cockell, S.J., Schneider, J.E., Mohun, T.J., Maehr, R., Kist, R., Peters, H.,
599 Bamforth, S.D., 2019. Pax9 is required for cardiovascular development and interacts with Tbx1
600 in the pharyngeal endoderm to control 4th pharyngeal arch artery morphogenesis,
601 Development, p. dev177618.

602 Randall, V., McCue, K., Roberts, C., Kyriakopoulou, V., Beddow, S., Barrett, A.N., Vitelli, F.,
603 Prescott, K., Shaw-Smith, C., Devriendt, K., Bosman, E., Steffes, G., Steel, K.P., Simrick, S.,
604 Basson, M.A., Illingworth, E., Scambler, P.J., 2009. Great vessel development requires biallelic
605 expression of Chd7 and Tbx1 in pharyngeal ectoderm in mice. J Clin Invest 119, 3301-3310.

606 Ryckebusch, L., Bertrand, N., Mesbah, K., Bajolle, F., Niederreither, K., Kelly, R.G., Zaffran, S.,
607 2010. Decreased levels of embryonic retinoic acid synthesis accelerate recovery from arterial
608 growth delay in a mouse model of DiGeorge syndrome. Circ Res 106, 686-694.

609 Sharma, B., Ho, L., Ford, G.H., Chen, H.I., Goldstone, A.B., Woo, Y.J., Quertermous, T.,
610 Reversade, B., Red-Horse, K., 2017. Alternative Progenitor Cells Compensate to Rebuild the
611 Coronary Vasculature in Elabela- and Apj-Deficient Hearts. Dev Cell 42, 655-666 e653.

612 Stoller, J.Z., Epstein, J.A., 2005. Cardiac neural crest, Seminars in Cell & Developmental
613 Biology, pp. 704-715.

614 Stothard, C.A., Mazzotta, S., Vyas, A., Schneider, J.E., Mohun, T.J., Henderson, D.J., Phillips,
615 H.M., Bamforth, S.D., 2020. Pax9 and Gbx2 Interact in the Pharyngeal Endoderm to Control
616 Cardiovascular Development. J Cardiovasc Dev Dis 7.

617 Taddei, I., Morishima, M., Huynh, T., Lindsay, E.A., 2001. Genetic factors are major
618 determinants of phenotypic variability in a mouse model of the DiGeorge:del22q11 syndromes.
619 PNAS 98, 11428-11431.

620 Tsao, C.W., Aday, A.W., Almarzooq, Z.I., Alonso, A., Beaton, A.Z., Bittencourt, M.S., Boehme,
621 A.K., Buxton, A.E., Carson, A.P., Commodore-Mensah, Y., Elkind, M.S.V., Evenson, K.R., Eze-
622 Nliam, C., Ferguson, J.F., Generoso, G., Ho, J.E., Kalani, R., Khan, S.S., Kissela, B.M.,
623 Knutson, K.L., Levine, D.A., Lewis, T.T., Liu, J., Loop, M.S., Ma, J., Mussolino, M.E.,
624 Navaneethan, S.D., Perak, A.M., Poudel, R., Rezk-Hanna, M., Roth, G.A., Schroeder, E.B.,
625 Shah, S.H., Thacker, E.L., VanWagner, L.B., Virani, S.S., Voecks, J.H., Wang, N.Y., Yaffe, K.,
626 Martin, S.S., 2022. Heart Disease and Stroke Statistics-2022 Update: A Report From the
627 American Heart Association. Circulation 145, e153-e639.

628 Van Mierop, L.H.S., Kutsche, L.M., 1986a. Cardiovascular anomalies in digeorge syndrome and
629 importance of neural crest as a possible pathogenetic factor, The American Journal of
630 Cardiology, pp. 133-137.

631 Van Mierop, L.H.S., Kutsche, L.M., 1986b. Cardiovascular anomalies in DiGeorge syndrome
632 and importance of neural crest as a possible pathogenetic factor. The American Journal of
633 Cardiology 58, 133-137.

634 Vitelli, F., Taddei, I., Morishima, M., Meyers, E., Lindsay, E.A., Baldini, A., 2002. A genetic link
635 between Tbx1 and fibroblast growth factor signaling. Development 129, 6.

636 Waddington, C.H., 1942. Canalization of development and the inheritance of the acquired
637 characters. Nature 150, 563-564.

638 Wang, X., Chen, D., Chen, K., Jubran, A., Ramirez, A., Astrof, S., 2017. Endothelium in the
639 pharyngeal arches 3, 4 and 6 is derived from the second heart field, Developmental Biology, pp.
640 108-117.

641 Warkala, M., Chen, D., Ramirez, A., Jubran, A., Schonning, M., Wang, X., Zhao, H., Astrof, S.,
642 2021. Cell-Extracellular Matrix Interactions Play Multiple Essential Roles in Aortic Arch
643 Development. Circ Res 128, e27-e44.

Yagi, H., Furutani, Y., Hamada, H., Sasaki, T., Asakawa, S., Minoshima, S., Ichida, F., Joo, K., Kimura, M., Imamura, S.-i., Kamatani, N., Momma, K., Takao, A., Nakazawa, M., Shimizu, N., Matsuoka, R., 2003. Role of TBX1 in human del22q11.2 syndrome, The Lancet, pp. 1366-1373.

Zhang, Z., 2006. Mesodermal expression of Tbx1 is necessary and sufficient for pharyngeal arch and cardiac outflow tract development, Development, pp. 3587-3595.

Zhang, Z., Baldini, A., 2008. In vivo response to high-resolution variation of Tbx1 mRNA dosage, Human Molecular Genetics, pp. 150-157.

Zhang, Z., Cerrato, F., Xu, H., Vitelli, F., Morishima, M., Vincentz, J., Furuta, Y., Ma, L., Martin, J.F., Baldini, A., Lindsay, E., 2005. Tbx1 expression in pharyngeal epithelia is necessary for pharyngeal arch artery development., Development (Cambridge, England), pp. 5307-5315.

Figure 1

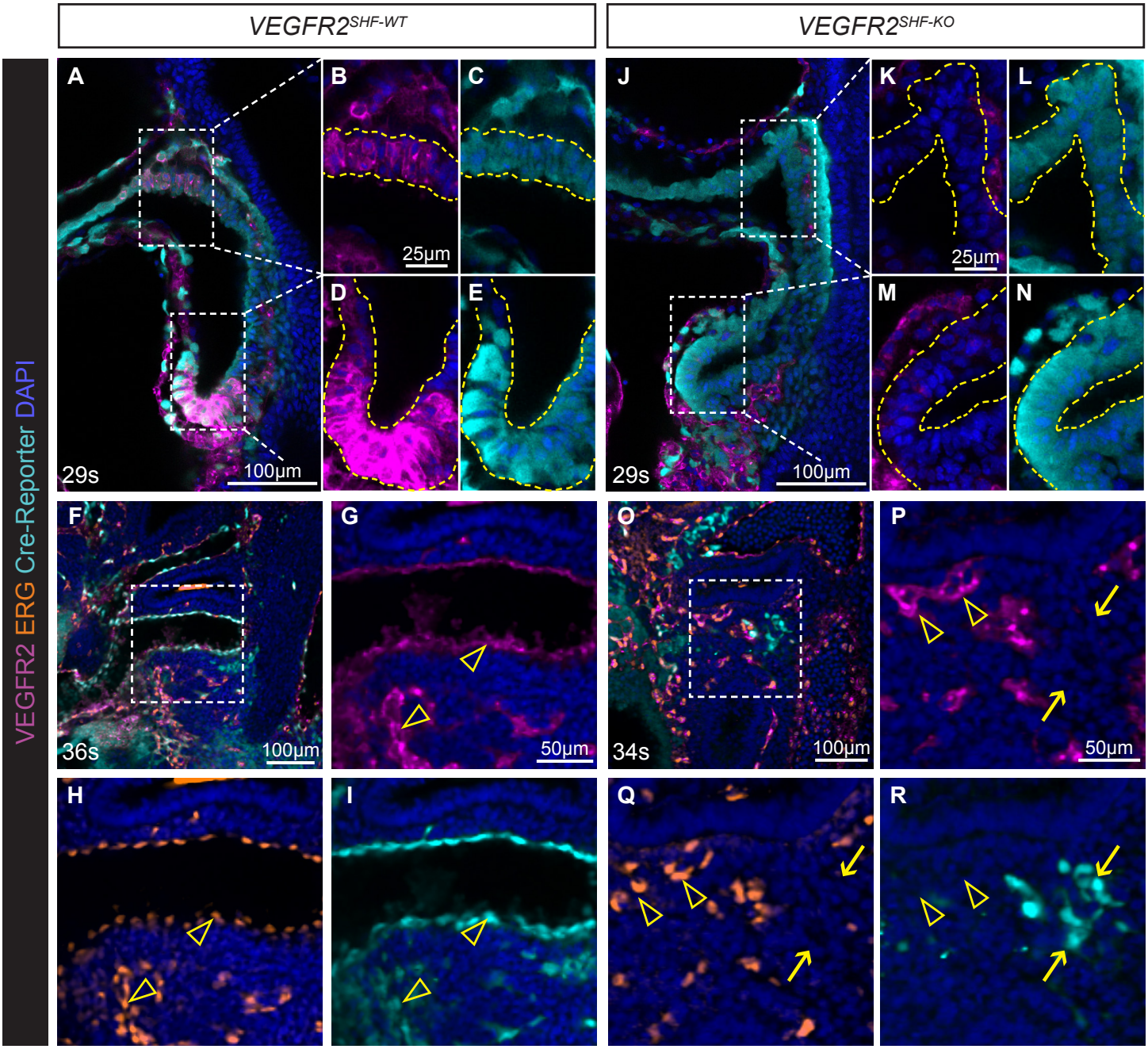

Figure 1. Efficient ablation of VEGFR2 in the second heart field (SHF) using *mef2c-AHF-Cre* mice.

Cre-lox recombination and immunofluorescent staining were used to trace *mef2c-AHF-Cre* lineage cells (cyan) when VEGFR2 (magenta) is conditionally ablated from the SHF in embryos. **(A-E)** Optical confocal sections of E9.5 *VEGFR2*$^{SHF\text{-}WT}$ embryos show VEGFR2+ cells in the anterior **(B-C)** and posterior **(D-E)** dorsal pericardial wall outlined in yellow. **(F-I)** PAA ECs in E10.5 *VEGFR2*$^{SHF\text{-}WT}$ embryos are derived from the SHF. The box in **F** is expanded in **(G-I)**. Arrowheads point to the co-expression of VEGFR2 (magenta), ERG (orange), and Cre-reporter (cyan) in the 4th pharyngeal arch endothelium. **(J-N)** Optical sections of E9.5 *VEGFR2*$^{SHF\text{-}KO}$ embryos show the absence of VEGFR2 expression in the anterior **(K-L)** and posterior SHF dorsal pericardial wall **(M-N)**, outlined in yellow. **(O-R)** PAA ECs in E10.5 *VEGFR2*$^{SHF\text{-}KO}$ embryos are derived from a non-SHF endothelium. The box in **O** is expanded in **(P-R)**. Arrowheads point to Cre-reporter negative endothelium. Arrows point to Cre-reporter+ VEGFR2-negative cells.

Figure 2

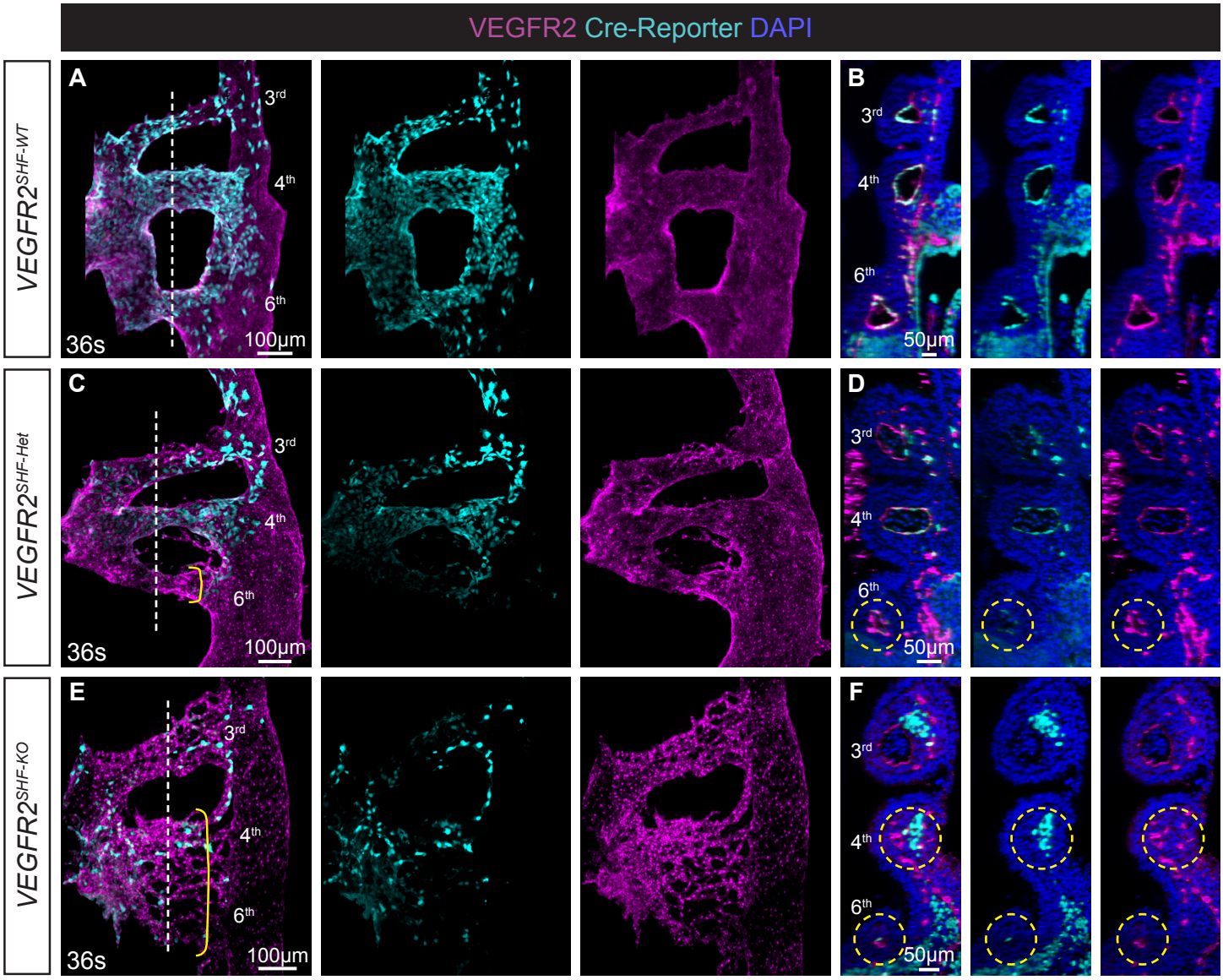
VEGFR2 Cre-Reporter DAPI
VEGFR2SHF-WT
VEGFR2SHF-Het
VEGFR2SHF-KO
A
B
C
D
E
F
3rd
4th
6th
36s
100µm
50µm

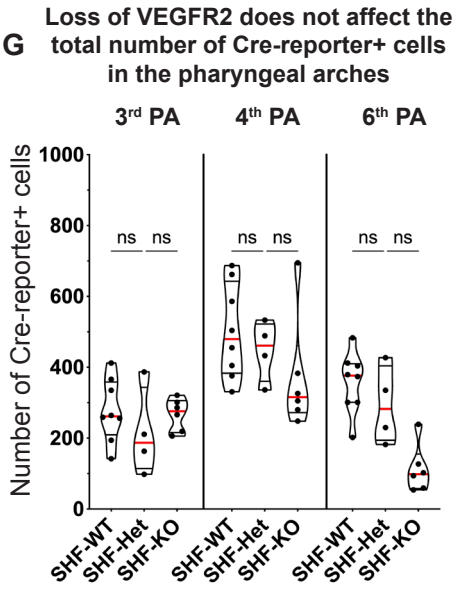
G
Loss of VEGFR2 does not affect the total number of Cre-reporter+ cells in the pharyngeal arches
3rd PA
4th PA
6th PA
Number of Cre-reporter+ cells
ns
SHF-WT
SHF-Het
SHF-KO

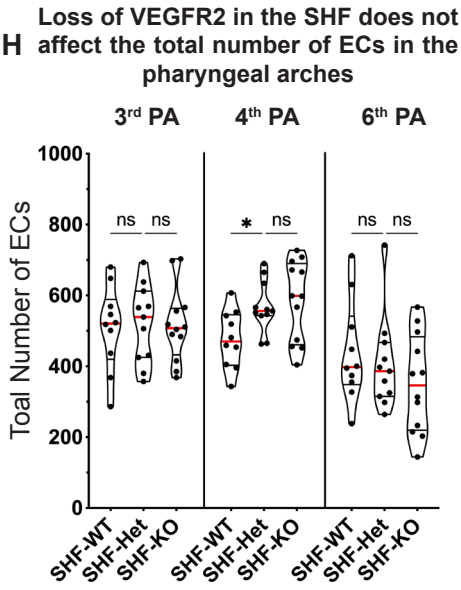
H
Loss of VEGFR2 in the SHF does not affect the total number of ECs in the pharyngeal arches
3rd PA
4th PA
6th PA
Toal Number of ECs
ns
*
SHF-WT
SHF-Het
SHF-KO

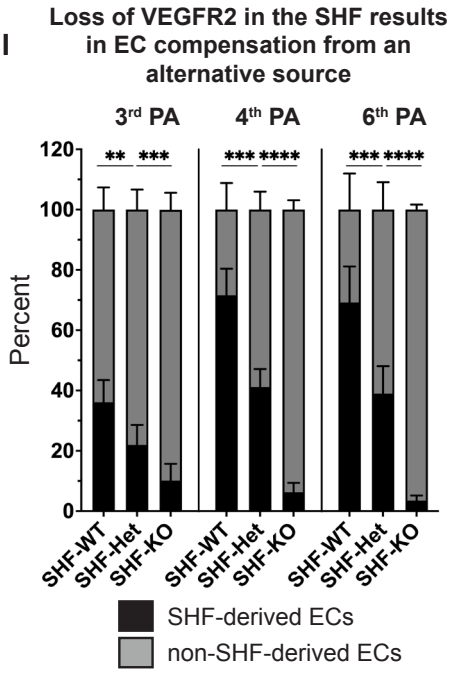
I
Loss of VEGFR2 in the SHF results in EC compensation from an alternative source
3rd PA
4th PA
6th PA
Percent
**
***
****
SHF-WT
SHF-Het
SHF-KO
SHF-derived ECs
non-SHF-derived ECs

Figure 2. VEGFR2 is required for SHF vascular progenitor contribution and PAA development. **(A-F)** WM-IF for VEGFR2 (magenta) and Cre-reporter (cyan), confocal imaging, and 3D reconstruction of E10.5 **(A)** *VEGFR2*$^{SHF\text{-}WT}$, **(C)** *VEGFR2*$^{SHF\text{-}Het}$, and **(E)** *VEGFR2*$^{SHF\text{-}KO}$ embryos. Yellow brackets highlight aberrant PAAs in **C, E**. Dashed lines mark the levels of coronal optical sections through the pharyngeal arches shown in **B, D,** and **F**. Dotted circles mark aberrant PAAs. **(G)** Quantification of SHF-derived cells in each pharyngeal arch. *VEGFR2*$^{SHF\text{-}WT}$ n = 10 arches, *VEGFR2*$^{SHF\text{-}Het}$ n = 4 arches, *VEGFR2*$^{SHF\text{-}KO}$ n = 6 arches. Each dot marks one pharyngeal arch. Horizontal red and black lines mark means and quartiles, respectively. **(H)** Quantification of total EC numbers in each pharyngeal arch. *VEGFR2*$^{SHF\text{-}WT}$ n = 10 arches, *VEGFR2*$^{SHF\text{-}Het}$ n = 12 arches, *VEGFR2*$^{SHF\text{-}KO}$ n = 12 arches. Each dot marks one pharyngeal arch. Horizontal red and black lines mark means and quartiles, respectively. **(I)** The proportion of Cre-reporter-positive ECs and Cre-reporter-negative ECs in each pharyngeal arch. Means ± SD are shown. *VEGFR2*$^{SHF\text{-}WT}$ n = 10 arches, *VEGFR2*$^{SHF\text{-}Het}$ n = 12 arches, *VEGFR2*$^{SHF\text{-}KO}$ n = 12 arches. Data were analyzed using two-way ANOVA with Tukey's correction for multiple testing; *$p \leq 0.05$ **$p \leq 0.01$, ***$p \leq 0.001$, ****$p < 0.0001$

Figure 3

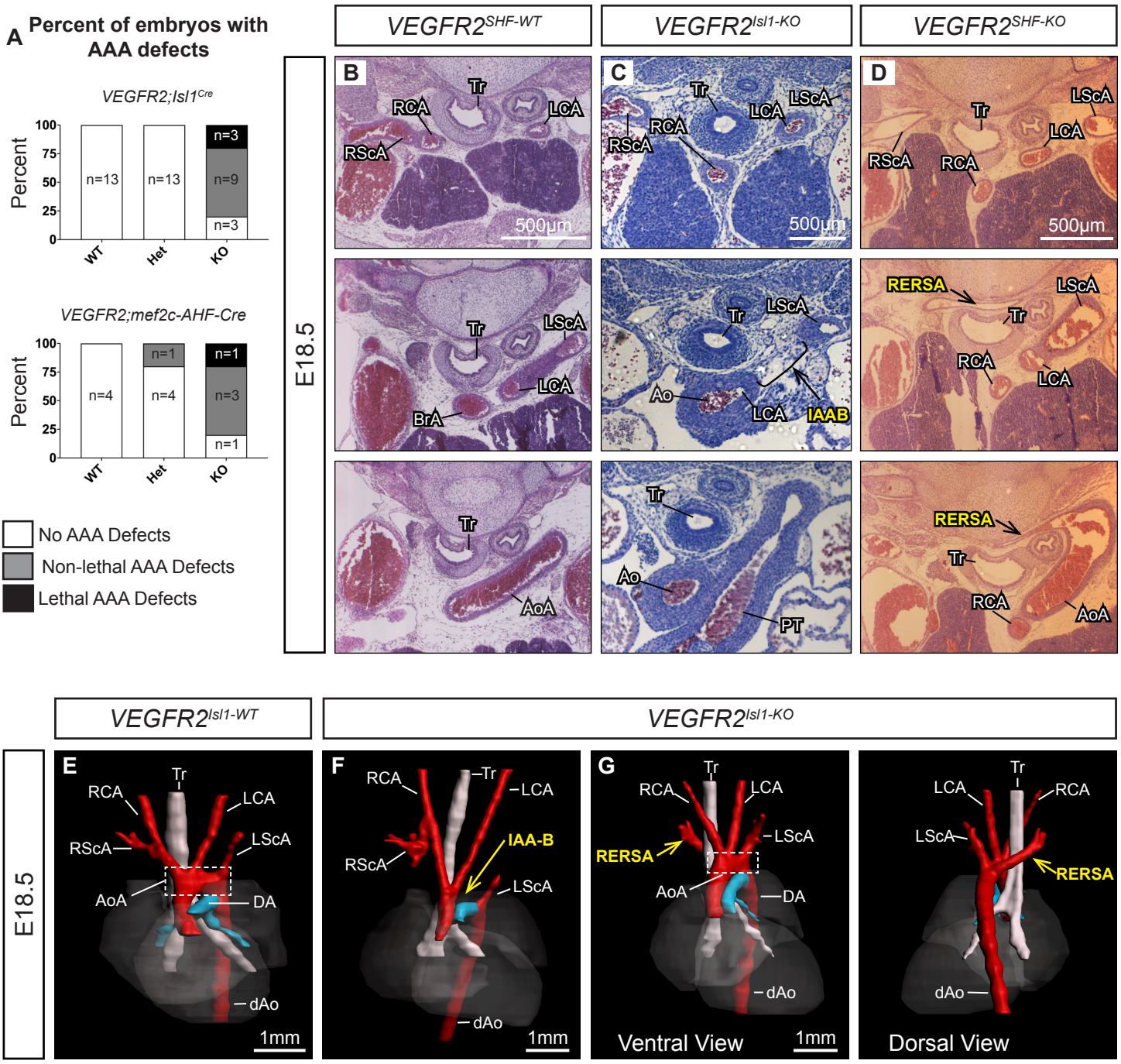

Figure 3. A threshold number of SHF-derived ECs is required for proper Aortic Arch Artery development.

(A) Percent of *VEGFR2;Isl1Cre* (*VEGFR2*$^{Isl1\text{-}WT}$, *VEGFR2*$^{Isl1\text{-}Het}$, and *VEGFR2*$^{Isl1\text{-}KO}$) and *VEGFR2;mef2c-AHF-Cre* (*VEGFR2*$^{SHF\text{-}WT}$, *VEGFR2*$^{SHF\text{-}Het}$, and *VEGFR2*$^{SHF\text{-}KO}$) embryos without AAA defects (white), non-lethal AAA defects (grey), or lethal AAA defects (black). n = the number of embryos with each phenotype. **(B-D)** Transverse sections of E18.5 embryos stained with Hematoxylin and eosin. **(B)** *VEGFR2*$^{SHF\text{-}WT}$ embryos. **(C)** IAA-B and **(D)** RERSA in *VEGFR2*$^{Isl1\text{-}KO}$ and *VEGFR2*$^{SHF\text{-}KO}$ embryos, respectively. **(E-G)** Micro-computed tomography of E18.5 *VEGFR2*$^{Isl1\text{-}WT}$ **(E)** and *VEGFR2*$^{Isl1\text{-}KO}$ **(F-G)** embryos. Arrows and text indicate examples of IAA-B **(F)** and aberrant RScA **(G)** in yellow. Dotted boxes highlight the position of a normal aortic arch. **Abbreviations:** RCA – right carotid artery; LCA – left carotid artery; RScA – right subclavian artery; LScA – left subclavian artery; BrA – brachiocephalic artery; AoA – aortic arch; PT – pulmonary trunk; DA – ductus arteriosus; dAo – descending aorta; TR – trachea; IAA-B – interrupted aortic arch type B; RERSA – retroesophageal right subclavian artery

Figure 4

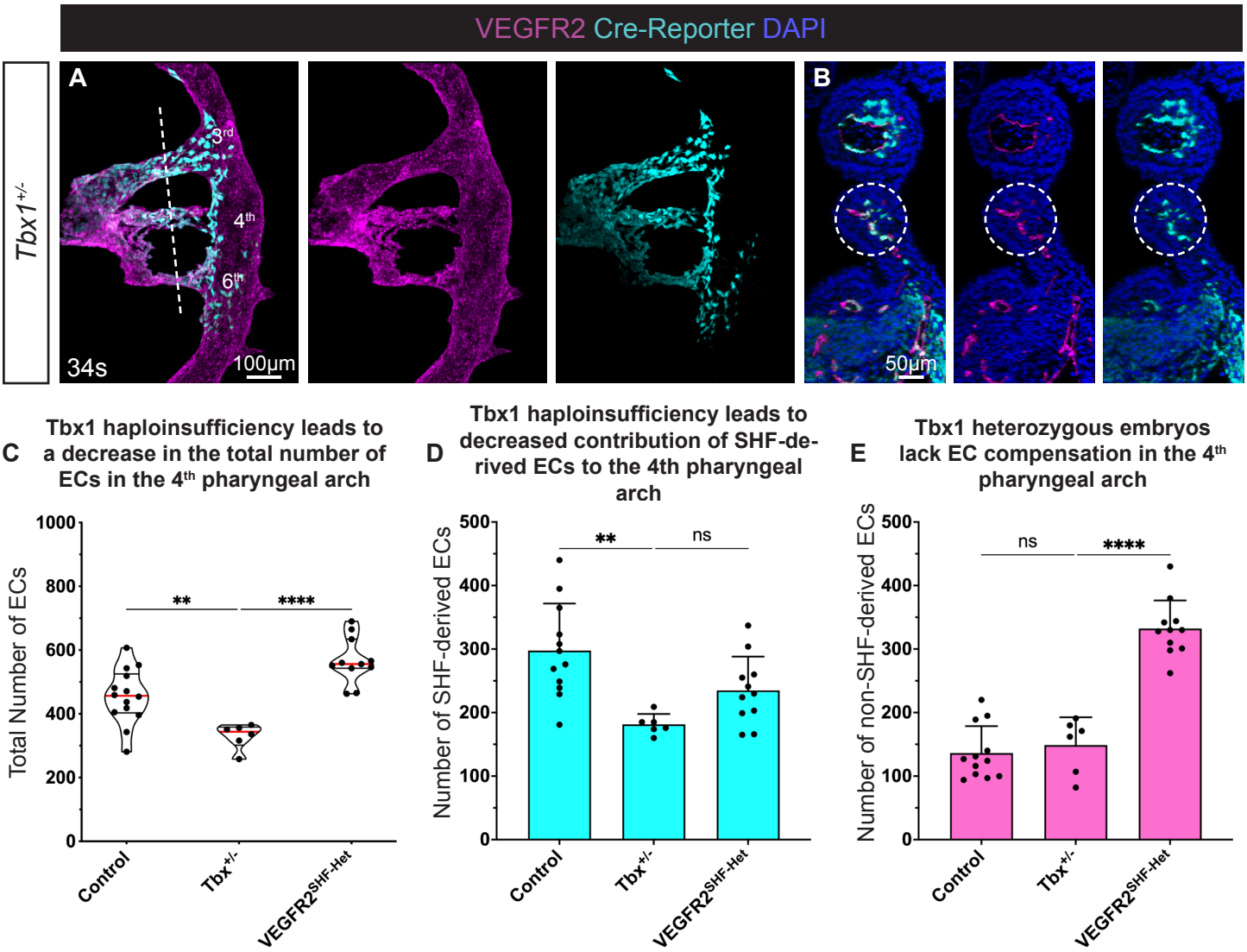

Figure 4. *Tbx1* regulates endothelial compensation and rescue of PAA development.
(A-B) WM-IF for VEGFR2 (magenta) and Cre-reporter (cyan) of an E10.5 *Tbx1*$^{+/-}$ embryo. **(A)** 3D reconstruction and **(B)** coronal optical sections show the incomplete formation of the 4th PAA (dotted circles) and that only a few non-SHF-derived ECs are present. **(C)** Quantification of ECs in the 4th pharyngeal arches of control (*mef2c-AHF-Cre*), *Tbx1*$^{+/-}$, and *VEGFR2*$^{SHF\text{-}Het}$ embryos. Each dot marks one pharyngeal arch. Horizontal red and black lines mark means and quartiles, respectively. **(D)** Quantification of the number of SHF-derived (Cre-reporter positive) ECs in the 4th pharyngeal arch. Error bars represent mean ± SD. **(E)** Quantification of the number of non-SHF-derived (Cre-reporter negative) ECs in the 4th pharyngeal arch. Error bars represent mean ± SD. Control n = 14 arches, *Tbx1*$^{+/-}$ n = 6 arches, *VEGFR2*$^{SHF\text{-}Het}$ n = 12 arches. Data were analyzed using one-way ANOVA with Tukey's correction for multiple testing; **$p \leq 0.01$, ****$p < 0.0001$

Figure 5

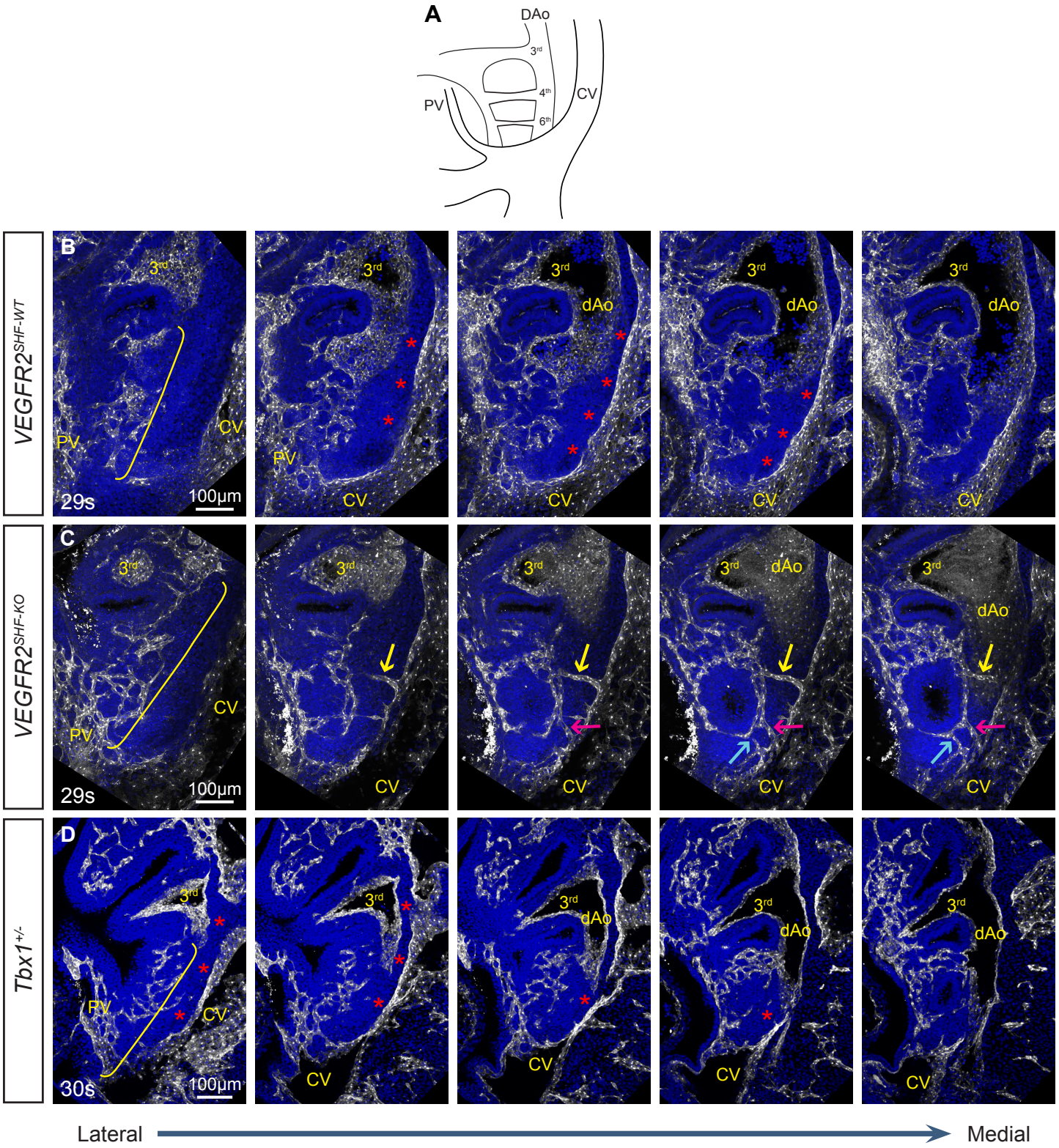

Figure 5. Ectopic sprouts from veins in the pharyngeal region of *VEGFR2^{SHF-KO}* are absent in *Tbx1$^{+/-}$* embryos.

(A) A schematic depiction of venous and arterial vasculature in the pharyngeal region of E9.5 embryos. dAo – dorsal aorta; CV – cardinal vein; PV – pharyngeal vein. **(B-D)** 20µm-thick serial sagittal optical sections through E9.5 *VEGFR2^{SHF-WT}* **(B)**, *VEGFR2^{SHF-KO}* **(C)**, and *Tbx1$^{+/-}$* **(D)** embryos from the lateral to the medial side. Yellow brackets in **B-D** mark pharyngeal endothelial plexus. Red stars mark absent venous sprouts in *VEGFR2^{SHF-WT}* **(B)** and *Tbx1$^{+/-}$* **(D)** embryos. Yellow, magenta, and cyan arrows follow sprouts from the CV to the pharyngeal arch vasculature in the VEGFR2SHF-KO embryos **(C)**.

Figure 6

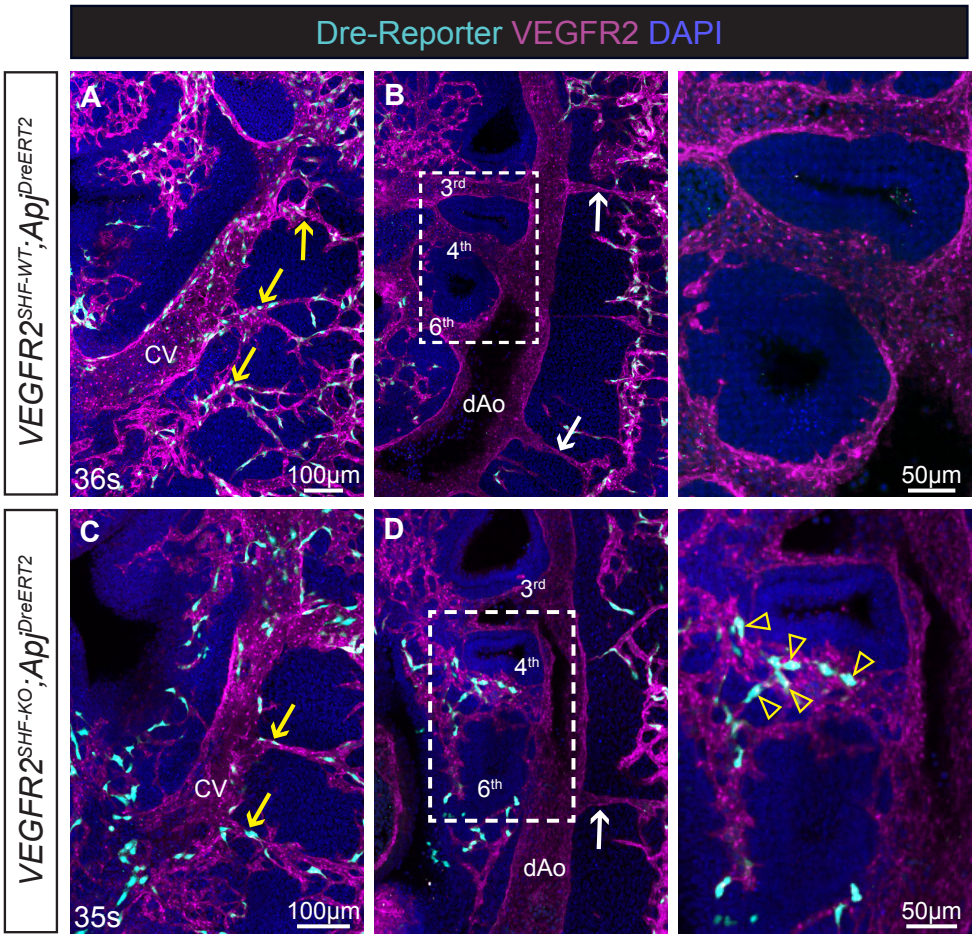
Dre-Reporter VEGFR2 DAPI
VEGFR2SHF-WT;ApjDreERT2
VEGFR2SHF-KO;ApjDreERT2
A
B
C
D
CV
dAo
3rd
4th
6th
36s
35s
100µm
50µm

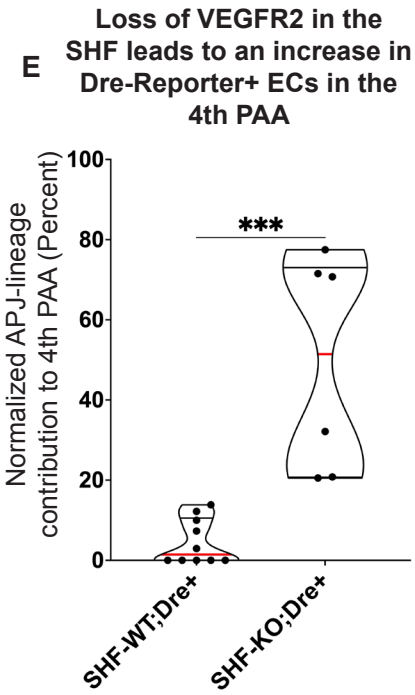
E
Loss of VEGFR2 in the SHF leads to an increase in Dre-Reporter+ ECs in the 4th PAA
Normalized APJ-lineage contribution to 4th PAA (Percent)
100
80
60
40
20
0
***
SHF-WT;Dre+
SHF-KO;Dre+

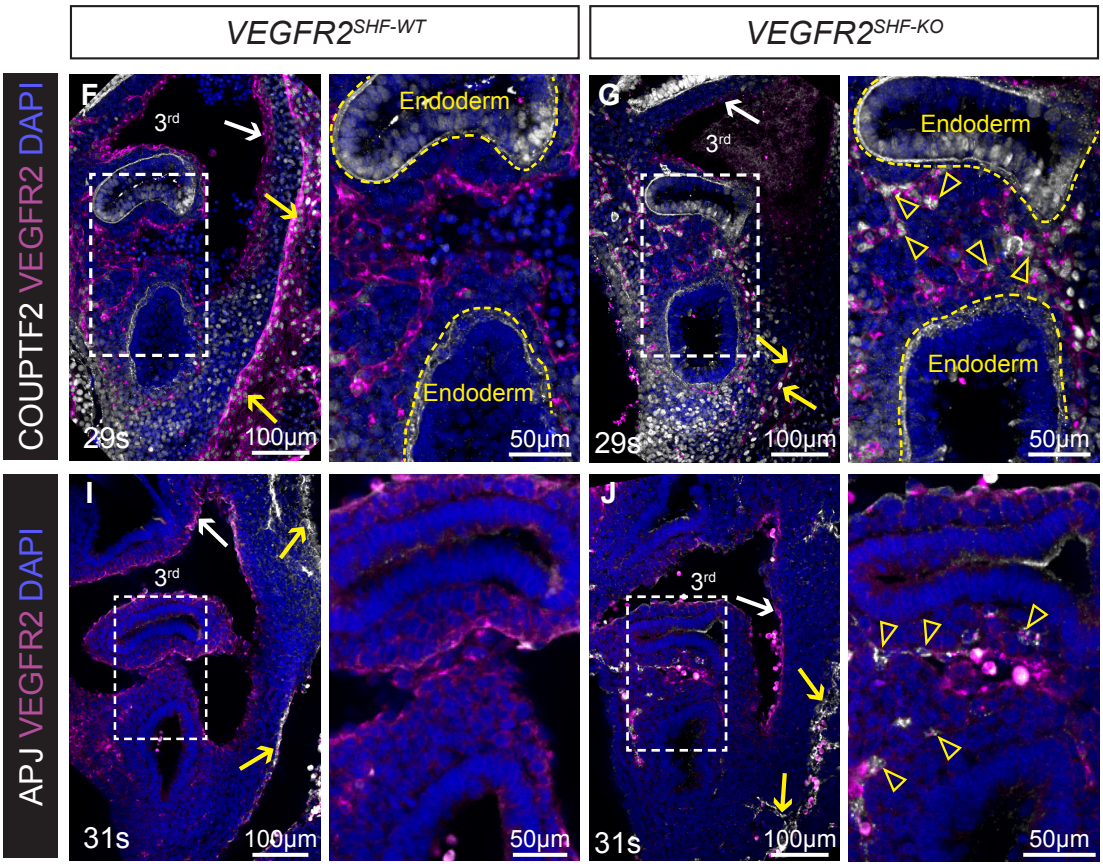
VEGFR2SHF-WT
VEGFR2SHF-KO
COUPTF2 VEGFR2 DAPI
APJ VEGFR2 DAPI
F
G
I
J
3rd
Endoderm
29s
31s
100µm
50µm

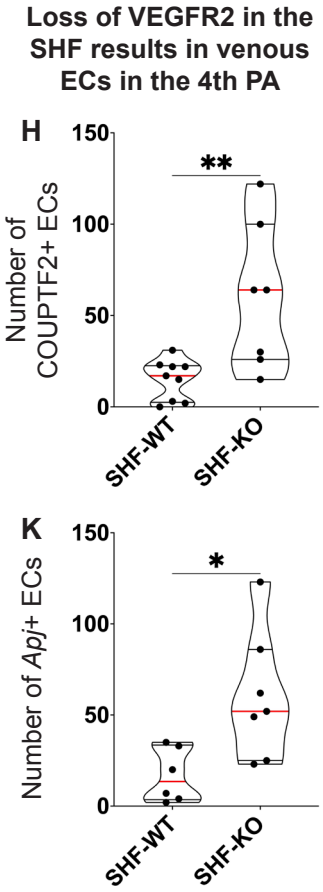
Loss of VEGFR2 in the SHF results in venous ECs in the 4th PA
H
Number of COUPTF2+ ECs
150
100
50
0
**
SHF-WT
SHF-KO
K
Number of Apj+ ECs
150
100
50
0
*
SHF-WT
SHF-KO

Figure 6. Angiogenic sprouting from veins gives rise to the compensatory endothelium that rescues PAA morphogenesis.

Dre-rox recombination was used to fate map cells of *Apj*-lineage in *VEGFR2*$^{SHF\text{-}WT}$ and *VEGFR2*$^{SHF\text{-}KO}$ embryos. Tamoxifen was injected at E9.5, and embryos were dissected at E10.5. **(A-D)** WM-IF staining detecting Dre-reporter (cyan) and VEGFR2 (magenta). 50μm-thick sagittal optical sections show *Apj-DreERT2* lineage labeling in the CV and intersomitic veins (yellow arrows) but not the dAo or intersomitic arteries (white arrows) of **(A)** *VEGFR2*$^{SHF\text{-}WT}$ and **(C)** *VEGFR2*$^{SHF\text{-}KO}$ embryos. Boxes in **B, D** are expanded in the panels on the right to show *ApjDreERT2* lineage labeled ECs in the 4th PAAs of *VEGFR2*$^{SHF\text{-}KO}$ embryos (arrowheads, **D**) but not in control, *VEGFR2*$^{SHF\text{-}WT}$ embryos **(B)**. **(E)** *VEGFR2*$^{SHF\text{-}KO}$ embryos have a higher percent contribution of *Apj*-lineage cells in the 4th PAAs. The number of *Apj*-lineage cells in arches was normalized by *ApjDreERT2* labeling efficiency (see Methods). Each dot marks one pharyngeal arch. Horizontal red and black lines mark means and quartiles, respectively. *VEGFR2*$^{SHF\text{-}WT}$ n = 10 arches, *VEGFR2*$^{SHF\text{-}KO}$ n = 6 arches. **(F-G)** WM-IF for COUPTF2 (magenta) and VEGFR2 (white) of E9.5 embryos. 20μm-thick sagittal optical sections: **(F)** *VEGFR2*$^{SHF\text{-}WT}$ and **(G)** *VEGFR2*$^{SHF\text{-}KO}$ embryos. Yellow arrows point to COUPTF2+ ECs in the CV. White arrows point to COUPTF2-negative ECs in 3rd PAA and dAo. Arrowheads point to COUPTF2+ ECs in the 4th PAA of *VEGFR2*$^{SHF\text{-}KO}$ embryo **(G)**. **(H)** Quantification of COUPTF2+ ECs in the 4th pharyngeal arches. Each dot marks one pharyngeal arch. Horizontal red and black lines mark means and quartiles, respectively. *VEGFR2*$^{SHF\text{-}WT}$ n = 9 arches, *VEGFR2*$^{SHF\text{-}KO}$ n = 7 arches. **(I-J)** Confocal optical sections. Single-molecule RNA fluorescence in situ hybridization for *Apj* mRNA (magenta) combined with immunostaining for VEGFR2 (white) of E10.0 embryos. Yellow arrows point to *Apj*+ ECs in the CV. White arrows point to *Apj*-negative ECs in 3rd PAA and dAo. **(K)** Quantification of *Apj*+ ECs in the 4th pharyngeal arches. Each dot marks one pharyngeal arch. Horizontal red and black lines mark means and quartiles, respectively. *VEGFR2*$^{SHF\text{-}WT}$ n = 6 arches, *VEGFR2*$^{SHF\text{-}KO}$ n = 7 arches. Data were analyzed using 2-tailed, unpaired Student's t-test; *$p \leq 0.05$, ** $p \leq 0.01$, ***$p \leq 0.001$.

Figure 7

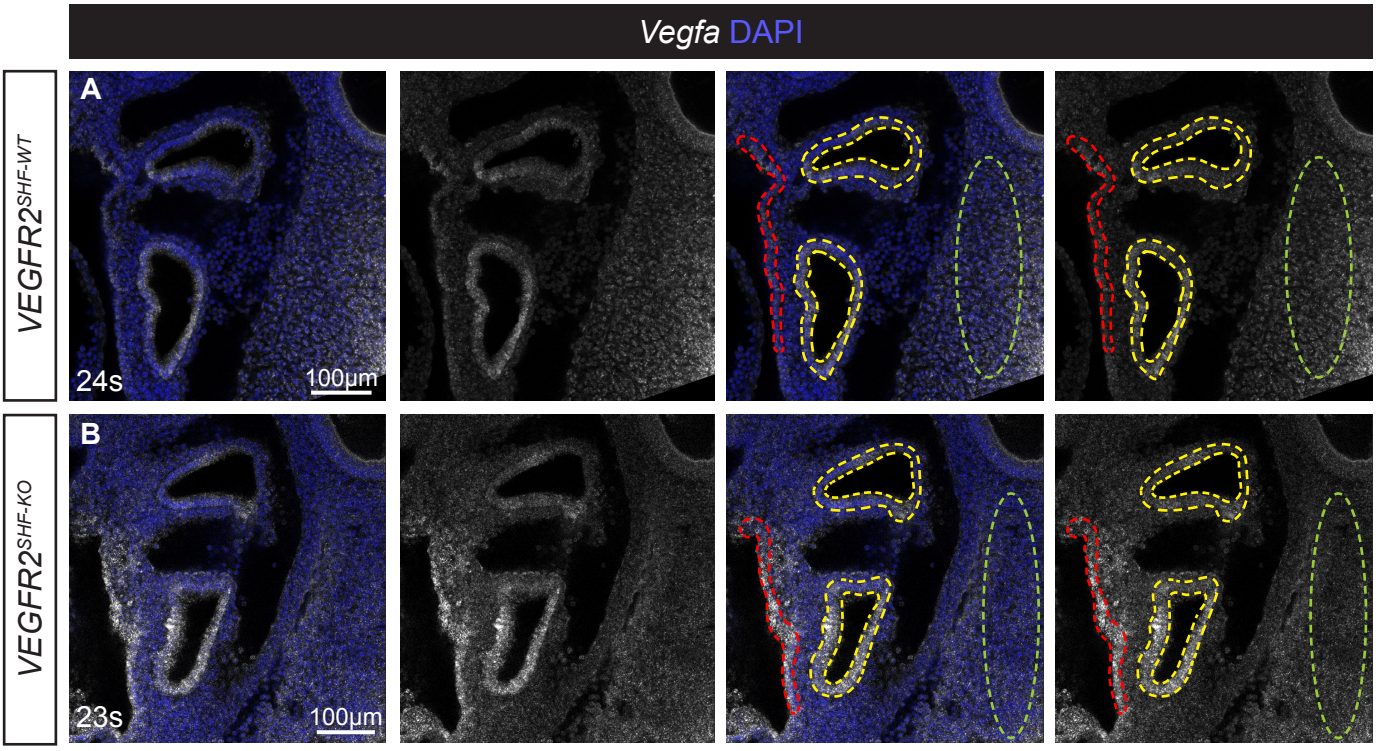

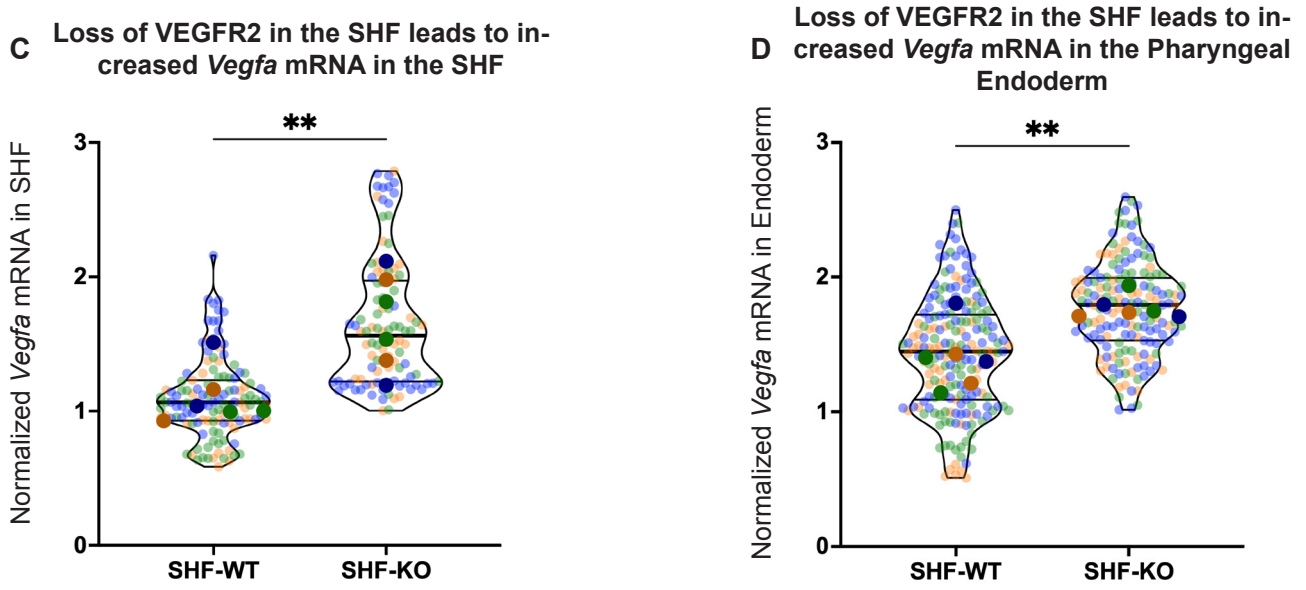

Figure 7. Loss of SHF-derived vascular progenitors increases *VEGFA* mRNA expression in the SHF and pharyngeal endoderm.

(A-B) Single-molecule RNA fluorescent in situ hybridization of E9.5 embryos detecting the expression of *VEGFA* (white) in the SHF (outlined in red) and pharyngeal endoderm (outlined in yellow). **(C)** Super plot of normalized mean fluorescence intensity of *VEGFA* mRNA in the SHF. **(D)** Super plot of normalized mean fluorescence intensity of *VEGFA* mRNA in the pharyngeal endoderm. The mean fluorescence intensity in the SHF and pharyngeal endoderm was normalized to the mean fluorescence intensity in the dorsal side of the embryo on the same optical section (outlined in green). Different colors in **C, D** mark different biological samples. Light-colored dots mark individual measurements in optical sections. Dark-colored dots mark the average of measurements per pharyngeal arch. Red lines mark means, and black lines mark quartiles. *VEGFR2*$^{SHF\text{-}WT}$ n = 6 arches, *VEGFR2*$^{SHF\text{-}KO}$ n = 6 arches. Data were analyzed using 2-tailed, unpaired Student's t-test; **$p \leq 0.01$.